UNIVERSITY OF HELSINKI REPORT SERIES IN PHYSICS

HU-P-D200

Effects of nuclear and electronic stopping power on ion irradiation of silicon-based compounds

Marie Backman

Division of Materials Physics
Department of Physics
Faculty of Science
University of Helsinki
Helsinki, Finland

ACADEMIC DISSERTATION

To be presented, with the permission of the Faculty of Science of the University of Helsinki, for public criticism in Auditorium XIV of the Main Building of the University of Helsinki, on December 15th 2012, at 12 o'clock noon.

HELSINKI 2012

ISBN 978-952-10-8086-9 (printed version)
ISSN 0356-0961
Helsinki 2012
Helsinki University Print (Unigrafia)

ISBN 978-952-10-8087-6 (PDF version)
http://ethesis.helsinki.fi/
Helsinki 2012
Electronic Publications @ University of Helsinki (Helsingin yliopiston verkkojulkaisut)

Marie Backman, **Effects of nuclear and electronic stopping power on ion irradiation of silicon-based compounds**, University of Helsinki, 2012, 49 p.+appendices, University of Helsinki Report Series in Physics, HU-P-D200, ISSN 0356-0961, ISBN 978-952-10-8086-9 (printed version), ISBN 978-952-10-8087-6 (PDF version)

Classification (INSPEC): A6180J, A6180M, A6185, A6146
Keywords (INSPEC): radiation effects, molecular dynamics method, energy loss of particles, nanostructured materials, silicon, germanium, silicon compounds

ABSTRACT

Ion irradiation is used to analyze and modify the structure of condensed matter. It can for instance be used to form and shape nanocrystals in solids. In research on materials for high radiation environments, ion beams function as a controlled source of irradiation for studying the basic mechanisms of ion-solid interactions and for analyzing the structure of materials by methods like Rutherford backscattering spectrometry. Understanding the fundamental processes that take place in a material under ion irradiation is important for all these applications of ion beams, and of great interest from a basic science point of view.

The mechanisms involved during ion irradiation-induced displacement of atoms in uniform bulk solids are fairly well understood and described in the literature, but many unresolved questions remain regarding the structural modification caused by electronic interactions, and the radiation response of materials with phase boundaries. Especially ion irradiation of nanomaterials is a topic that is under active research. The short-lived collision cascades caused by energetic ions in solids cannot be studied in experiments and are therefore often modeled in computer simulations. Such simulations can give a host of valuable information about processes that occur in nature. It is necessary to validate simulation results by either some other computational method, or ideally by experiments.

Ions lose energy by elastic collisions with the atomic nuclei as well as to the electronic system through excitation and ionization. Both energy loss mechanisms – nuclear and electronic stopping – can cause modifications to the structure of the material. In this thesis, molecular dynamics simulations are carried out in close collaboration with experimental scientists in order to study the effects of nuclear and electronic stopping during ion irradiation on nanoclusters and bulk materials.

The amorphization of germanium and silicon nanocrystals in silica under ion irradiation is studied in simulations. The amorphization dose of nanocrystals is much lower than for bulk materials and it is furthermore found to depend on the size of the nanocrystals. The inelastic thermal spike model is explored as a method of incorporating electronic stopping effects into molecular dynamics. The simulations predict that local heating due to electronic stopping contributes to irradiation damage

in both nanocrystals in silica and bulk silica. In silicon carbide, high electronic stopping is found to recrystallize irradiation damaged samples. Molecular dynamics simulations of inelastic thermal spikes support the hypothesis that the observed recrystallization is induced by local heating due to electronic stopping.

We need a combination of computer simulations and experimental observations to explain many of the complex processes that take place during ion irradiation. The results in this thesis give insight into some experimentally observed phenomena of the effect that nuclear and electronic energy loss have in materials, but especially the research on combined effects is still in its infancy and further progress can be expected in the near future.

Contents

1 INTRODUCTION

Charged particle beams have been one of the most successful experimental tools for probing the structure of matter. Indeed, it was early experiments on charged alpha particles incident on thin gold foils, in the famous Geiger-Marsden experiment [1], that helped establish the Rutherford planetary model of the atom in 1911 [2], which Niels Bohr improved on in 1913 [3]. Today, a hundred years after these break-throughs in describing the structure of the atom, physicists within the CERN collaboration use colliding particle beams to explore what the universe is made of and how it works. In the hundred years that have passed after the Geiger-Marsden experiment, ion beam technology has advanced tremendously and played a major part in the development of the modern computer through the doping of silicon for integrated circuits.

While Bohr might be better known for developing the quantum physics-based model of the atom, he was also instrumental in developing the theory for how charged particles interact with matter [4, 5, 6], or stopping theory as we might call it today. Since then, Bethe, Fermi, Lindhard and many others have improved the models describing ion energy loss. Computational models, like binary collision approximation and molecular dynamics simulations, have proved to be indispensable tools in the study of ion-solid interactions. Understanding of the processes that take place as ions interact with matter have been crucial for the controlled use of ion beams in technological processes.

The most important industrial process involving ion beams is arguably ion implantation doping of silicon in manufacturing the tiny integrated circuits that make up modern computers. While other methods of doping have been used, ion beams is the prevailing method in today's semiconductor industry [7]. The basic mode of operation in the microchip is the same as in the 1970s. There are research efforts into replacing the conventional microchip with alternatives with optical functionality. Semiconductor nanocrystals in silica, formed by ion implantation and annealing, is a proposed material for such optoelectronical circuits [8].

In addition to the use in materials modification and analysis, ion irradiation has long been used for experimentally simulating radiation effects by neutrons in materials for nuclear reactors [9]. The higher dose rate of ion beams (in displaced atoms per second) provides a means for estimating the radiation effects from many years of neutron bombardment in a controlled experiment lasting only hours or minutes. An additional advantage of replacing neutrons with ions is that activation of the irradiated sample is avoided. Potential materials for future fusion reactors are also submitted to irradiation testing prior to their use [10].

The interaction of energetic ions with living tissue is an important research topic due to the exploratory use of ion beams in cancer treatment. So called particle therapy is a method in which ion beams are

used instead of x-rays for damaging cancer cells [11, 12]. In x-ray therapy, healthy tissue is also exposed to a significant radiation dose since x-rays lose energy continuously in solid matter. Charged atoms, on the other hand, deposit most of their energy in a narrow volume around the depth where the atoms come to rest in the material. By tuning the ion energy, the depth range can be tuned to the exact location of the tumor to avoid damage to healthy tissue. Particle therapy is already today in use in a few hospitals, but so far the observed advantages have not been substantial enough to motivate the copious increase in cost of using ion beams instead of x-rays [12].

Ion irradiation has evolved into one of the most versatile tools used in materials science, and particularly in nanoscience [13]. Research goes into analyzing destructive effects of particle irradiation as well as into modifying materials properties and creating new materials. In all of these applications, we need a grasp of the processes that occur in the material. The studies in this thesis concern the ion irradiation of embedded nanoclusters in silica and other silicon-based compounds. Specifically, computer simulations are used for investigating the roles of nuclear and electronic stopping in the structural changes that take place under ion irradiation. The results will elucidate the atomistic origin of experimentally observed ion irradiation phenomena.

2 PURPOSE AND STRUCTURE OF THIS STUDY

The purpose of this study is to improve our understanding of how nuclear and electronic stopping of ions affect irradiation damage in materials. This is done by molecular dynamics simulations of ion irradiation in silicon-based compounds. The results will give insight into the fundamentals of ion irradiation and help explain experimental results.

The structure of the thesis is as follows. In this section, the six publications are summarized and the author's contributions are presented. In section 3, an introduction to nanocrystals in solids is given. Some fundamental aspects of energy loss by ions in matter are presented in section 4. Section 5 concerns the computational methods used in the work, followed by the results on ion irradiation of nanocrystals in section 6 and of silicon-based bulk compounds in section 7. In section 8, the conclusions are presented.

2.1 Summaries of the original publications

Publication I: Amorphization of Ge nanocrystals embedded in amorphous silica under ion irradiation, F. Djurabekova, M. Backman, O. H. Pakarinen, K. Nordlund, L. Araujo, and M. Ridgway,

Nucl. Instr. Meth. Phys. Res. B **267**, 1235-1238 (2009).

The amorphization of 4 nm Ge nanocrystals in silica under ion irradiation is studied in experiments and atomistic simulations. The structural disorder of the irradiated nanocrystals is assessed in EXAFS measurements. The unirradiated nanocrystals are partly disordered due to their high surface-to-volume ratio, and become amorphous at a much lower dose than needed for bulk Ge.

Publication II: Amorphization of Ge and Si nanocrystals embedded in amorphous SiO_2 by ion irradiation, M. Backman, F. Djurabekova, O. H. Pakarinen, K. Nordlund, L. L. Araujo, and M. C. Ridgway, *Phys. Rev. B* **80**, 144109 (2009).

Ion irradiation of different sizes of Si and Ge nanocrystals in silica reveals a size dependent amorphization dose in both simulations and experiments. Even the sample with the largest sizes of nanocrystals, average diameter 9 nm, becomes amorphous at a dose that is lower than that for the bulk material. The nanocrystals become amorphous but retain their spherical shape and are not dissolved in the matrix.

Publication III: Contribution of Electronic Energy Deposition to the Atomic Cascade Damage in Nanocrystals, M. Backman, F. Djurabekova, O. H. Pakarinen, K. Nordlund, and M. Toulemonde, *MRS Symposium Proceedings* **1264**, 1264-BB02-07 (2010).

The effect of electronic energy loss on ion irradiation damage is studied in Ge nanocrystals in silica. The electronic excitations are assumed to give heat to the lattice through electron-phonon coupling; this phenomenon is modeled by the inelastic thermal spike model. The local heating along the trajectory of the ion is found to have a significant enhancing effect on the collision cascade damage.

Publication IV: Cooperative effect of nuclear and electronic stopping on ion irradiation damage in silica, M. Backman, F. Djurabekova, O. H. Pakarinen, K. Nordlund, Y. Zhang, M. Toulemonde, and W. J. Weber, *J. Phys. D: Appl. Phys.* **45**, 505305 (2012).

Silica has a large band gap and is susceptible to lattice modification by electronic stopping of heavy ions. Ion irradiation in the intermediate energy range, in which nuclear and electronic stopping are of similar magnitude, is studied in MD simulations of Au irradiation in silica. The inelastic thermal spike induces damage also below the threshold for latent track formation and therefore contributes significantly to irradiation damage by collision cascades.

Publication V: Combined experimental and computational study of the recrystallization process induced by electronic interactions of swift heavy ions with silicon carbide crystals, A. Debelle, M. Backman, L. Thomé, W. J. Weber, M. Toulemonde, S. Mylonas, A. Boulle, O. H. Pakarinen, N. Juslin, F. Djurabekova, K. Nordlund, F. Garrido, and D. Chaussende, *Phys. Rev. B* **86**, 100102(R) (2012).

The response of radiation damaged 3C-SiC to swift heavy ion irradiation is studied by experiments and simulations. The electronic excitations produce defect recovery in both a fully amorphous layer and a partially disordered region. In the fully amorphous layer, recrystallization takes place at the amorphous-to-crystalline interface. The partially disordered layer shows a decrease in defects over the whole damage thickness. The good agreement between simulations and experiments suggests that the experimentally observed defect recovery is a result of inelastic thermal spike annealing.

Publication VI: Molecular dynamics simulations of swift heavy ion induced defect recovery in SiC, M. Backman, M. Toulemonde, O. H. Pakarinen, N. Juslin, F. Djurabekova, K. Nordlund, A. Debelle, and W. J. Weber, *Comp. Mater. Sci.* **67**, 261 (2013).

In this publication, the effect of swift heavy ion irradiation on different model damage states in SiC is studied in molecular dynamics simulations. The inelastic thermal spike induces recovery of Frenkel pairs up to 10 nm from the ion trajectory. The damage level in a disordered and amorphous layer, respectively, is found to decrease with the number of overlapping thermal spikes.

2.2 Author's contribution

The author carried out most of the simulations and their analysis in publications **I** and **II** and contributed to the writing of the Introduction and Methods sections in publication **II**. The experimental work for publications **I** and **II** was done by Dr. Araujo and Dr. Ridgway at the Australian National University in Canberra, Australia. The simulations in publications **III**-**VI** were carried out by the author, with the exception of the inelastic thermal spike calculations which were done by Dr. Toulemonde at CIMAP in Caen, France, and the binary collision approximation calculations for publication **IV** which were done by Dr. Djurabekova at the University of Helsinki, Finland. The experimental part of publication **V** was carried out by Dr. Debelle and colleagues at CSNSM and Université Paris-Sud in Orsay, France. The author wrote the major part of publications **III**, **IV**, and **VI** and the part concerning the simulations of publication **V**.

3 NANOCRYSTALS IN SOLIDS

Nanoscience is highly interdisciplinary and connects fields such as physics, chemistry, materials science and biomedicine. It deals with materials that at least in some dimension are 1-100 nm in size. Discoveries of novel properties that appear in materials as they reach the nanoscale have spurred an enormous research interest in nanomaterials. Two specific properties of matter at the nanoscale make it unique from any other size scale. First, nanostructures have a very large ratio of surface atoms to bulk atoms, which makes surface properties proportionally more important. Second, the nanoscale is small enough to exhibit quantum mechanical effects. For instance, in semiconductor nanoclusters, the band gap is found to vary with the size of the nanocluster [14]. These two characteristics – a large number of surface atoms and quantum effects – make the properties of nanoscale material different from bulk matter and sometimes even size dependent. In the following, we will focus on nanocomposites of disperse nanocrystals in a solid matrix, which are interesting because of the optical properties that arise at the nanoscale.

3.1 Properties of embedded nanocrystals

Free nanoparticles can be used in certain applications, especially medical, but for the majority of applications, bulk realizations of nanoscale phenomena are preferable. For this purpose, nanostructures can be embedded in a bulk matrix (as in Fig. 1) to make use of the nanoscale properties, or explore new properties that arise due to the interface between the nanostructure and the bulk matrix. While the properties of such nanocomposites are a question of fundamental scientific interest, most research is motivated by potential applications in electronics and optoelectronics.

Embedded nanocrystals are also interesting from a purely mechanical point of view; so called *nanocomposites* – a bulk material reinforced by nanostructures – can exhibit a considerable increase in hardness compared to the hardness predicted by the rule of mixtures. The nanostructures hinder dislocation motion and grain boundary sliding, which create plastic deformation. This mechanism makes the material harder, but less ductile. High toughness is, however, equally important although more difficult to achieve, but in nanocomposite design, parameters such as materials, nanocluster size and distribution can be tweaked to achieve an optimal balance between hardness and toughness [15]. Films containing dispersed nanoclusters should be distinguished from nanocrystalline films; the former has the advantage of being more ductile than the latter [16] if an amorphous matrix is used for ductility while the hardness is kept high by the inclusion of nanoclusters [17]. The inclusion of metal nanoparticles in a ceramic matrix takes advantage of the hardness due to covalent bonds in combination with ductility given by metallic bonds [18]. One of the most studied nanocomposites are oxide

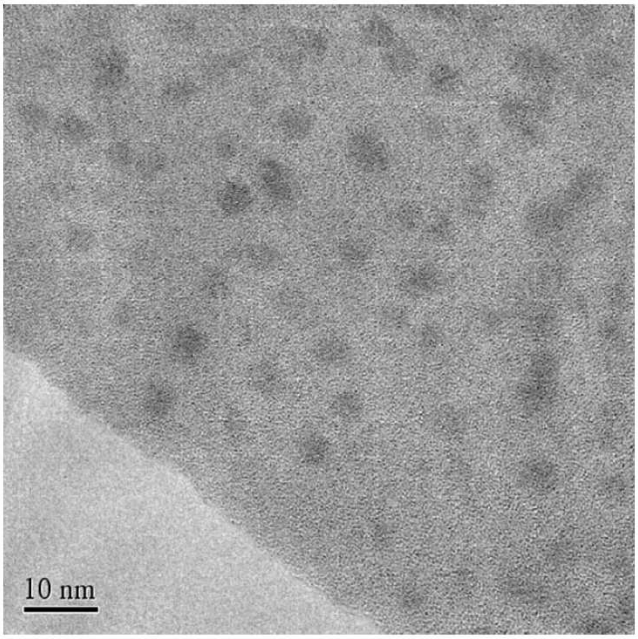

Figure 1: TEM image of germanium nanocrystals in silica formed by ion implantation and annealing at 1060 °C for 1 hour, from publication **I**. Thermal annealing promotes segregation of the implanted germanium, which forms spherical nanocrystals in the silica sample.

dispersion strengthened (ODS) steels, which contain oxide nanoclusters that increase the resistance to irradiation damage and make them promising materials for nuclear energy applications [19, 20] (Section 6).

Nevertheless, the most remarkable properties of nanostructures are electronic and optical. Nanosized clusters have indeed been used for their optical properties for more than 2000 years. The Lycurgus Cup, which was dated to around 300 AD, is a famous example of pottery that contains embedded gold and silver nanoparticles, which make the color of the cup change depending on whether light is transmitted from the inside of it or reflected from its surface [21]. The formation of nanoclusters was probably happenstance, but the fascinating consequence was not. The electronic properties are different on the nanoscale. In semiconductors the band gap of nanocrystals is found to be size dependent due to quantum confinement of electrons [22]. In metals on the other hand, surface effects are predominant and alter the electronic properties, the most notable example being the surface plasmon resonance in noble metal nanoparticles [23]. Today, a hot topic of research is silicon nanocrystals in amorphous SiO_2 (silica), which, despite the indirect band gap of bulk silicon, can emit light.

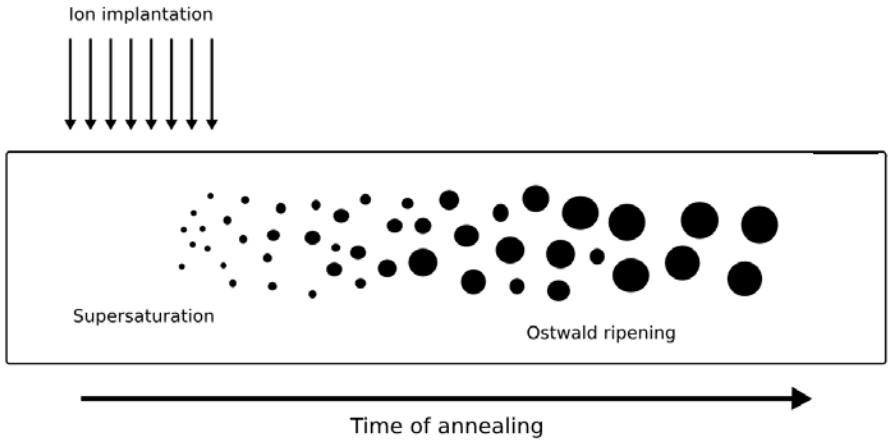

Figure 2: Formation of nanocrystals in solids by ion implantation and thermal annealing. An element that is immiscible in the matrix is implanted and segregation is enhanced by the elevated temperature. As time goes on, the nanocrystals will grow larger at the expense of smaller nanocrystals. This development is called Ostwald ripening.

3.2 Si nanocrystals in silica

Silicon is the basis of the semiconductor industry, but has the disadvantage of being an indirect band gap semiconductor. This property makes it unsuitable for optical devices since optical transitions require the assistance of phonons. The pursuit for smaller and faster electronic devices, however, led researchers to try to find ways of combining silicon with optoelectronics. For example, the speed of integrated circuits can be enhanced if optical communication, already used for long-distance communication between computers, was used instead of electrical circuits. One step in that direction was the discoveries of light emittance from silicon with a nanosized microstructure.

In 1990, Canham [24] demonstrated that porous Si can emit visible light and not long after, Shimizu-Iwayama *et al.* [25] attained photoluminescence in Si nanocrystals in silica. The origin of the photoluminescence is subject of much debate; the only consensus seems to be that luminescence in embedded nanocrystals is *not* due to quantum confinement [26, 27]. Nevertheless, this nanocomposite was proposed as a material for memory devices [28], optical switches [29], solar cells [30], and optical memories [31, 32], to name a few potential applications.

It is worth mentioning that one reason for the interest in embedded Si nanocrystal systems stems from that they are highly compatible with existing semiconductor technology both in terms of materials and fabrication methods. Embedded nanoparticles can be formed through segregation of an immiscible material in a bulk matrix [33]. The precursor can be a thin layer of the nanocrystal species or a supersaturated solution, prepared by for instance co-deposition or ion implantation into the matrix [34]. Free energy minimization leads to the nucleation and growth of spherical nanoclusters of the

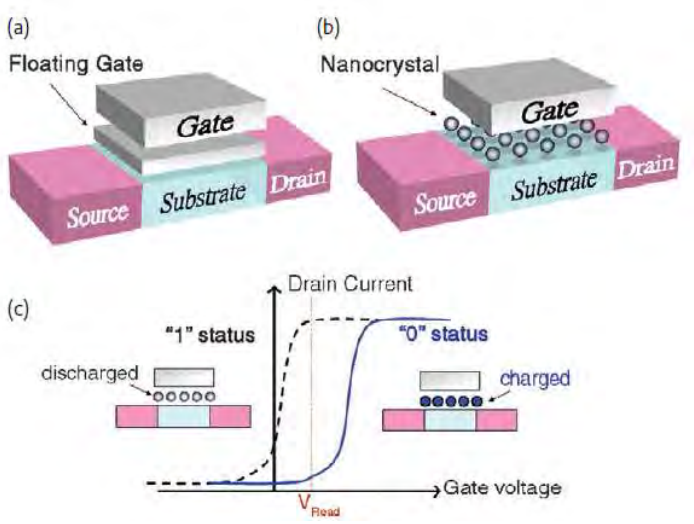

Figure 3: The structure of (a) floating gate memory and (b) nanocrystal memory. Nanocrystal memories in (b) have been proposed as alternatives to the conventional floating gate memories depicted in (a), in an effort to scale down the size of memories. The memory status of the nanocrystal memory is shown in (c). (Reprinted from Ref. [34] with permission from Elsevier.)

immiscible substance and the process is sped up by thermal annealing (Fig. 2). Analogous to the growth of free nanoclusters, large clusters grow at the expense of small ones in a process that is called *Ostwald ripening*. While different synthesis routes have been used, the advantage of ion implantation is that it is a mature technology that already is used on a large scale in the semiconductor industry [7].

Since their invention, integrated circuits have seen a steady decrease in size accompanied by an increase in performance. We are, however, approaching the so-called interconnect bottleneck, as the increased number of transistors per chip requires such a large number of interconnected wires, that the communication time becomes speed-limiting [35]. Replacing the electrical communication by optical communication, perhaps with the help of semiconductor nanocrystals, has been suggested as a solution to the interconnect bottleneck [31, 32, 36].

Nanocrystals have been proposed as a solution to the problem of fabricating smaller floating gate memories [37, 34], using the design shown in Fig. 3. At certain sizes, the floating gates cannot be scaled down in size without loss in performance as the gate oxide starts to leak charge [38]. Nanocrystals inside an oxide can function as discrete traps for charges. The storage of charge in a nanocrystal layer offers an advantage compared to conventional floating gates, where charge is stored in one location and a single weak spot can compromise the function of the device [37]. The main benefit is the reduction in oxide thickness due to so-called Coulomb blockade [39]. The first exploratory products with nanocrystal memories were recently introduced [40, 41, 42].

In conclusion, embedded nanocrystals combine the unique properties of nanostructures with a bulk sample that makes technological applications possible. Their characteristics depend on the size and size distribution of nanocrystals, on their concentration, and of course on the characteristics of the nanocrystal and host materials. While much of the interest in these materials currently comes from basic research, the industrial application of embedded nanocrystals as a solid state memory shows that commercialization of materials with embedded nanocrystals is viable.

4 NUCLEAR AND ELECTRONIC STOPPING

This chapter will scratch the surface of energy loss by charged particles in matter, a subject that has been studied and written about by numerous physicists. The following treatment of nuclear and electronic stopping power is inspired by a number of texts on the topic [6, 43, 44, 45, 9].

The *stopping power* of a medium for a particle is a measure of the average energy loss per unit path length of the particle due to interactions with the atoms in the medium. It is consequently defined as

$$S = \frac{\mathrm{d}E}{\mathrm{d}x} \tag{1}$$

where E is the kinetic energy of the particle and x distance along the particle trajectory in the medium. By the definition in equation 1, we see that S is strictly speaking a force and not a power. The term *stopping force* has indeed been proposed [46], but the term stopping power is deep-rooted in the field and broadly accepted. To first order, the stopping power of a target for an ion depends on the ion energy E and atomic number Z_1, as well as on the density and the atomic number Z_2 of the target element(s).

The atomistic origin of energy loss is in interactions between the ion and target atoms. The interaction mechanisms by which the ion can lose energy are (i) excitation or ionization of the electrons in the target (electronic energy loss), (ii) elastic collisions with the nuclei of target atoms (nuclear energy loss), and (iii) radiative emission of energy. One can thus divide the total stopping power into three independent parts,

$$S_{\mathrm{tot}} = S_{\mathrm{electronic}} + S_{\mathrm{nuclear}} + S_{\mathrm{radiative}}. \tag{2}$$

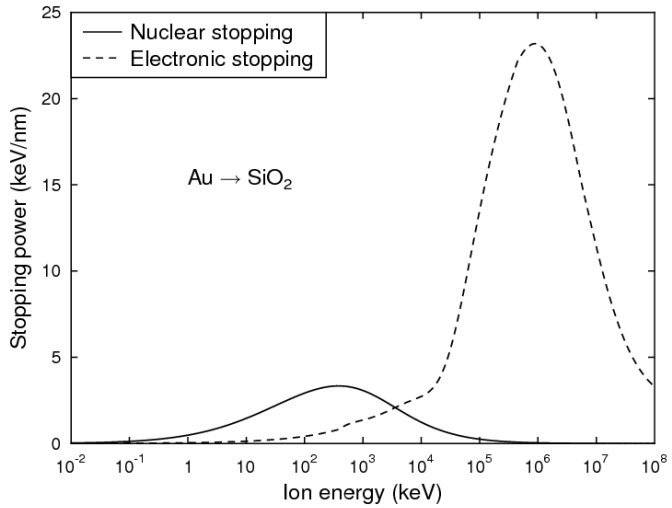

Figure 4: Nuclear and electronic stopping powers of SiO_2 for Au ions obtained from SRIM [47]. The stopping power is the loss in energy of an ion per unit path length. Note that the x-axis is logarithmic.

At projectile energies well below the speed of light, $S_{\text{radiative}}$ can be neglected. This leaves us with electronic and nuclear energy loss, which will be discussed in detail in the following sections. As an example, Fig. 4 shows the electronic and nuclear energy loss for gold ions in silicon dioxide. In order to theoretically describe average energy losses, we need the microscopic concept of reaction cross section σ. If, for some reaction, we know the cross section for transfer of energy T from projectile with initial energy E, $\sigma(E,T)$, then the average energy transfer $\bar{T}$ is given by

$$\bar{T} = \frac{\int T\sigma \mathrm{d}T}{\int \sigma \mathrm{d}T} \tag{3}$$

and the mean free path between reactions is $\lambda = \sigma/N$, where N is the number density. These two quantities, $\bar{T}$ and λ, now give the energy loss by

$$\frac{\mathrm{d}E}{\mathrm{d}x} = \frac{\bar{T}}{\lambda} = \frac{\int T\sigma(E,T)\mathrm{d}T}{\int \sigma(E,T)\mathrm{d}T} \cdot N \int \sigma(E,T)\mathrm{d}T = N \int T\sigma(E,T)\mathrm{d}T. \tag{4}$$

Closely connected to stopping power is the total range of ions, that is, the path length of the ions in the target until they come to rest. A more useful quantity is the projected range perpendicular to the surface, or how deep into the target the ions have penetrated. The total range can be calculated if the stopping power as a function of energy is known, and if continuous energy loss is assumed.

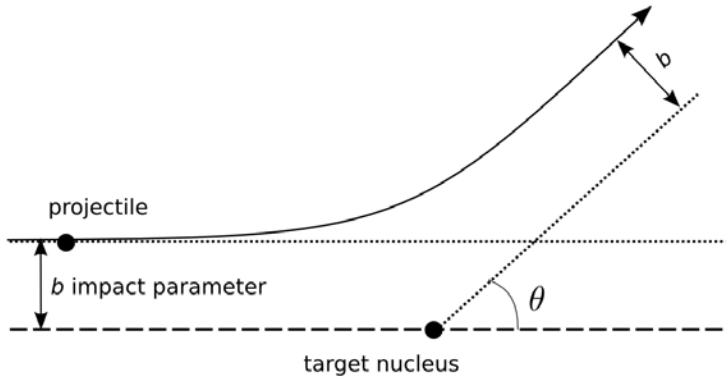

Figure 5: Scattering of an energetic ion by a stationary atom in the laboratory frame.

Knowledge of stopping powers and ranges is important in both ion beam analysis and materials modification, not to mention in radiation shielding. We can estimate the penetration depth (or projected range) of implanted atoms if the instantaneous energy losses are known. Ion beam analysis methods such as Rutherford backscattering spectrometry measure the ion energy after backscattering and one needs to correct for different energy losses depending on the path length inside the target [48]. Another application that can be mentioned is particle therapy for treatment of cancer [12]. While x-rays deposit energy continuously in tissue, ion beam energies can be tailored to have a desired end of range, and therefore deposit most of the energy, at the depth of the tumor.

4.1 Nuclear energy loss

The theoretical framework behind nuclear stopping starts from the mathematical description of a classical collision between two charged particles. We will attempt to find an expression for the scattering cross section as a function of the energy for the incoming projectile, from which the stopping power can be calculated using equation 4. This problem is illustrated in Fig. 5.

As a first step, we aim to find the energy transferred from projectile to atom in a collision. In an elastic collision between an ion with mass m_1 and kinetic energy E_0 and a stationary particle of mass m_2, energy and momentum will be conserved. By transforming the problem to the center of mass (CM) frame and evaluating the scattering interaction (see *e.g.* [43, 9]), we find that the energy T lost by the projectile to the atom depends on the scattering angle θ in the following way:

$$T = \frac{4E_0 m_1 m_2}{(m_1+m_2)^2}\sin^2\frac{\theta}{2} = T_{\max}\sin^2\frac{\theta}{2}. \tag{5}$$

Note that this formula is valid only at non-relativistic velocities. As expected, the maximum transfer of energy occurs in a head-on collision ($\theta = \pi$) and when the projectile and atom are of equal mass. This result is valid for any type of interaction, but if we assume spherically symmetric potentials $V(r)$, we can write the classical scattering integral as

$$\theta = \pi - 2b \int_{r_{\min}}^{\infty} \frac{\mathrm{d}r}{r^2 \left[1 - \frac{V(r)}{E_c} - \frac{b^2}{r^2}\right]}, \tag{6}$$

where b is the impact parameter, E_c the CM energy and r the radial polar coordinate connecting the projectile to the atom. Equations 5 and 6 give θ as a function of T and b as a function of θ, respectively. These relations can now be used for calculating the differential cross section

$$\sigma(E_i, T)\mathrm{d}T = 2\pi b \mathrm{d}b$$

$$\sigma(E_i, T) = 2\pi b \frac{\mathrm{d}b}{\mathrm{d}\theta}\frac{\mathrm{d}\theta}{\mathrm{d}T} \tag{7}$$

$$\sigma(E_i) = \int \sigma(E_i, T)\mathrm{d}T \tag{8}$$

which gives us the stopping power as defined in equation 4.

The biggest hurdle for determining the stopping power is finding the repulsive interaction potential $V(r)$. At high energies and small interatomic separations, $V(r)$ reduces to repulsive Coulomb interaction between the nuclei. At intermediate separations, which is the most relevant region for ion bombardment, there is screening of the charges which makes this region very complicated to describe accurately. In order to model the interactions we need to find an appropriate screening function $\Phi(r)$ for the Coulomb potential,

$$V(r) = \frac{Z_1 Z_2 e^2}{4\pi\varepsilon_0 r}\Phi(r/a), \tag{9}$$

where a represents a screening length, often dependent on the atomic numbers Z, and r/a is called the reduced radius. The use of the reduced radius r/a makes the function $\Phi(r/a)$ in many classical interatomic potentials independent of Z_1 and Z_2.

One of the most used screening functions for modelling atomic collisions is the one proposed by Ziegler, Littmark and Biersack [43]. The authors used Hartree-Fock and local density approximation calculations to find the interatomic potential between a large number of randomly chosen element pairs and fitted screening functions to the data. They furthermore determined a screening length a that made the screening functions for the individual pairs of potentials collapse onto one line, to good approximation. This approach allowed them to fit the so called universal screening function to the individual reduced screening functions:

$$\Phi(x) = 0.1818e^{-3.2x} + 0.5099e^{-0.9423x} + 0.2802e^{-0.4029x} + 0.02817e^{-0.2016x} \quad (10)$$

$$a = \frac{0.8854a_0}{Z_1^{0.23} + Z_2^{0.23}}. \quad (11)$$

For brevity, r/a is substituted by x in equation 10. A good approximation to most stopping powers can be obtained by using the universal interatomic potential in the scattering integral and calculating the differential energy transfer cross section as outlined above. If a more accurate repulsive potential is needed, for instance in computer simulations of ion irradiation, *ab initio* calculations for the specific atom-target pair can be used [49]. In *ab initio* or electronic structure calculations, one solves the Schrödinger equation numerically for a system of interest. Exact solutions can only be obtained for very small systems, and many different sets of approximations need to be introduced to extend the method to larger systems. The most popular variant of *ab initio* calculations in condensed matter physics is density functional theory (DFT), in which one postulates that (i) all the properties of the system are determined by the electron density $\rho(\mathbf{r})$ and (ii) the correct electron density minimizes the total energy of the system [50]. We will occasionally refer to *ab initio* methods, but an extensive review is beyond the scope of this thesis.

The elastic scattering of atoms by an energetic ion causes collision cascades that can modify or create damage to the structure of the material. The atoms displaced by the ion are called primary knock-on atoms or primary recoils. Primary recoils with high enough energy to displace other atoms create subcascades along the ion trajectory. This is illustrated in Fig. 6. Light ions often create small isolated subcascades. Subcascades from heavy ions, on the other hand, can be very large and involve hundreds of atoms; this is called a heat spike or thermal spike [51]. Note that in this thesis, the term *inelastic thermal spike* or *thermal spike* will be used for denoting the local heating that can be induced by an ion with high electronic energy loss (section 5.3).

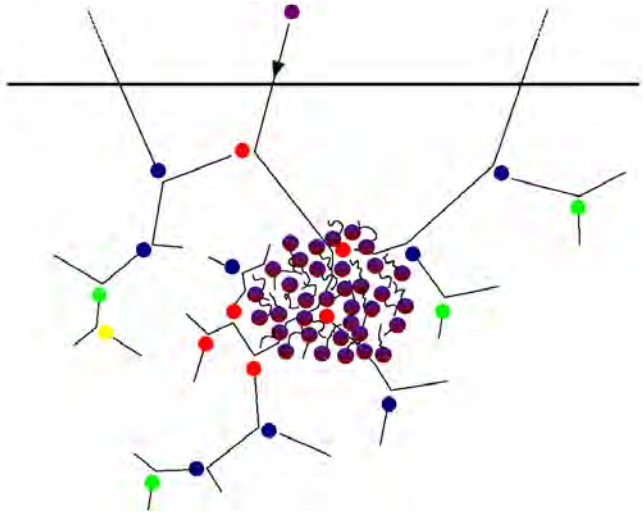

Figure 6: Illustration of a heat spike and linear collision cascade during ion irradiation of a solid. The red, blue, green, and yellow circles represent primary, secondary, tertiary and quaternary recoils, respectively. The purple circles illustrate a heat spike, where the cascade is dense and multiple collisions occur in a small volume. Outside the heat spike, atoms move in straight lines between collisions. Picture from [52].

4.2 Electronic energy loss

In general, despite the wide attention given to radiation damage due to nuclear stopping, most of the ion energy is lost to electronic stopping. The interactions between a charged particle and bound electrons are very complex and therefore rather difficult to describe theoretically. That is to say, electrons in the target can both collide elastically with a projectile and be excited or ionized, and the same processes can take place for the electrons of the energetic ion [43].

The electronic energy loss for ions has a peak at intermediate energies (Fig. 7). At high projectile energies, the ion is stripped of its electrons and the situation can to a good approximation be seen as Coulomb scattering between the ion and electrons in the target. The stopping power is consequently found by solving the scattering integral (equation 6) for the Coulomb potential (equation 9) without screening, and using NZ_2 as the electron density, which gives

$$\left(\frac{\mathrm{d}E}{\mathrm{d}x}\right)_e = NZ_2\pi\frac{Z_1^2\varepsilon^4}{E}\frac{m_1}{m_e}\ln\left(\frac{\gamma E}{I}\right), \tag{12}$$

where γ is the kinematic factor $4m_1m_2/(m_1+m_2)^2$ and $\bar{I}$ is the average ionization energy. Equation 12, which arises only from analysis of elastic collisions, is almost identical to the Bethe equation [53] for electronic stopping at high energies, except for the absence of a factor 2 that arises when a quantum

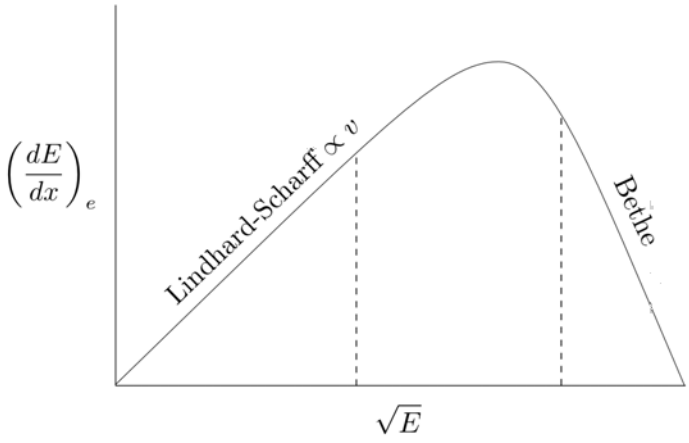

Figure 7: Electronic stopping regimes. The electronic stopping for slow ions is proportional to the velocity of the ion, while for fast ions the electronic stopping decreases with increasing kinetic energy.

mechanical treatment is carried out. The Bethe formula gives a good approximation for the electronic stopping at relatively high energies but below the regime in which relativistic effects need to be accounted for.

At low projectile energies, the ion is close to neutral and the conduction electrons contribute more to the electronic energy loss. This is because lower energies are needed to excite such electrons compared to inner shell electrons, for which the closest energy levels might be filled. Simple considerations regarding an elastic collision between a projectile and an electron and the proportion of electrons available for excitation [9] give that the stopping power at low energies is proportional to the ion velocity:

$$\left(\frac{\mathrm{d}E}{\mathrm{d}x}\right)_e = 8\sigma_e N \left(\frac{m_e}{m_1}\right)^{1/2} E^{1/2} = kE^{1/2}. \tag{13}$$

This expression gives a reasonable approximation in the low ion energy regime. The lower limit of energy at which electronic energy loss is present can be estimated as the projectile energy for which the maximum energy that can be transferred is lower than the lowest possible excitation (*i.e.* the band gap in non-metals).

The electronic stopping for heavy ions is of practical importance later in this work in the simulations of electronic energy deposition by swift heavy ions. The knowledge on stopping of heavy ions is limited, partly due to the difficulties in describing such a complicated many-electron process theoretically. Consequently, the SRIM predictions for heavy ions are significantly less accurate than those for lighter ions. Sigmund [54] has suggested the theory of reciprocity as a tool for assessing the plausibility of

electronic stopping cross sections for heavy ions. In brief, it states that the interaction cross section for an ion-atom pair should be invariant under exchange of atomic species at ion velocities below the Bohr velocity (25 keV/u). This principle is used in publication **IV** for deducing the Au stopping cross section in SiO_2 by the Si and O stopping cross sections in Au.

4.3 Interplay between electronic and nuclear stopping

Studies of irradiation effects are wont to focus on either displacement damage due to nuclear stopping, or the effects of intense electronic excitations and ionization due to a swift heavy ion. This distinction is sensible, considering that in most situations one or the other of electronic and nuclear stopping is bound to overshadow the other. From a fundamental science point of view it is, nevertheless, intriguing to consider what, if any, the combined effect of electronic and nuclear energy loss is. Many researchers have speculated on a synergy between electronic and nuclear damage processes, but experimental or theoretical data on such interactions are scarce. Only very recently have theoreticians used time dependent density functional theory to study radiation effects [55, 56, 57, 58, 59], hence, we can expect more progress in the near future.

A starting point for the research on interaction between electronic and nuclear stopping were the studies of ion irradiation in silica [60, 61] that showed that there are two different damage regions. (The reason for choosing silica is that the material has a large band gap, which makes ionization and excitation effects more noticeable.) From the surface and inward there is an even distribution of damage due to the electronic energy loss, while at the end of the ion range there is a damage peak caused by atomic collisions. The authors saw the fact that that the damage in the two areas were annealed at different temperatures as evidence for two separate damage mechanisms.

Nagata *et al*. studied light ion irradiation of silica and found that the electronic energy loss anneals the cascade damage caused by the same ion [62]. The same effect, a decrease in the damage efficiency due to electronic effects, has also been found in metals [63, 64]. Since the relative magnitudes of the electronic and nuclear energy loss varies with the ion energy, experimental studies on the damage as a function of ion energy have given insight into the interplay between the two damage mechanisms. Jaque and Townsend [65] measured luminescence in silica during ion irradiation at different energies and assumed an annealing effect due to the electronic excitations. On the other hand, Toulemonde *et al.* [66] recently found a synergy between the damage due to the nuclear and electronic stopping in silica. It is thus not yet established what the role of electronic effects during ion irradiation is, or even by what mechanism it would interact with the collision cascade.

It was recently shown that swift heavy ion irradiation can anneal damage *previously* created by collision cascades due to lower energy ions. This result was for instance demonstrated in SiC by Rutherford backscattering spectrometry [67, 68]. There is also an account of the same phenomenon in InP [69]. Given the different response of different materials, and the controversy regarding the origin of the observed materials modification by electronic stopping (Section 5.3), there are many open questions in this area. In publications **III-VI**, we study and try to explain some of these phenomena using atomistic simulations.

5 COMPUTATIONAL METHODS

Computer simulations have been an invaluable tool in research on ion-solid interactions. Even fairly simple models can give great insight into fundamental processes. The most prominent example might be the early binary collision simulations by Robinson and Oen in 1963 [70], which were among the first to show that the passage of ions in crystals can be strongly influenced by channeling effects. Computer models not significantly more advanced than those used by Robinson and Oen are today in continuous use by ion beam scientists in the SRIM computer program [71].

An important use of computer simulations is for predicting radiation damage in materials in different high radiation environments. Molecular dynamics (MD) simulations are for instance used extensively for testing the radiation tolerance of materials for fission [9] and fusion [72] reactors. Today, it is common to combine different computational methods for studying radiation effects in what is called multiscale modelling. For instance, *ab initio* calculations can provide the structures and energies of defects needed for constructing an interatomic potential for MD simulations of collision cascades. The number and types of defects created in the cascades can serve as input in methods that can model defect diffusion on longer time scales, like kinetic Monte Carlo or rate theory. The following sections will present the computational methods used in this work for studying the ion irradiation effects in nanocrystals and bulk materials.

5.1 Binary collision approximation

Binary collision approximation (BCA) simulations of ion scattering in a material is used daily by both experimental and computational materials scientists in the computer code SRIM [71]. The BCA approach is also used in the GEANT4 framework [73], which is a code used in high energy, nuclear, and particle physics and most notably within the CERN collaboration. As the name suggests, the binary collision approximation treats the passage of an ion through matter as a series of discrete

collisions between two atoms. Only at ion energies greater than roughly 1 keV can many-body effects be neglected, hence, other methods are better suited at low energies (see Section 5.2 about molecular dynamics). For high energies, however, the binary collision approximation has been a useful tool for estimating for instance ion implantation profiles.

In the following, we will outline the basic principles of BCA simulations [74, 43]. The collisions of the ion are treated as classical elastic collisions using the scattering integral, equation 6, but for computational efficiency an approximative analytic expression, or so called Magic Formula [75], is used. As discussed in Section 4.1, the scattering is governed by the interaction potential, but the potential can in practical cases not be known analytically and have to be estimated using for instance *ab initio* methods. The nuclear energy loss is lost in discrete amounts in collisions with the target atoms. The electronic energy loss is treated as a friction force and subtracted continuously from the ion energy.

BCA simulation codes for simplicity often assume an amorphous target, and thereby neglect effects of crystal structure such as focusing and channeling. This is found to be a decent approximation as long as the correct atomic density is used. The density of the material under study is invoked through the free flight distance λ. In SRIM, the free flight distance is fixed to the interatomic distance at low projectile energies, and at high energies, at which low angle scattering dominates, it is longer and energy dependent [43]. For each collision, a random impact parameter and azimuthal angle compared to the initial direction are generated. Since the impact parameter gives the scattering angle and the energy transferred to the knocked on atom (equations 5 and 6), these parameters uniquely define the trajectories of the projectile and knocked-on atom. An important parameter in BCA calculations is the threshold displacement energy, which is subtracted from the energies of knocked-on atoms that can then undergo further random collisions. Because the method relies on random numbers, it can be called Monte Carlo BCA.

Usually, BCA simulations are used for producing an ensemble of random ion histories from which averaged quantities like the ion ranges and displacements per atom in the material can be deduced. In publication **IV**, we used the BCA code CASWIN [76] for generating input for cascade simulations of MeV energy ions in MD. The code CASWIN assumes an amorphous target, and the recoil element is chosen randomly according to the relative concentration of the species in the simulated compound. Full BCA cascade simulations were carried out in a realistic sample size down to a cut-off energy for validity of the binary collision approximation, which we chose to be 1 keV. Such a cut-off method has been used earlier in Ref. [77]. The recoil positions and velocities served as input in the MD simulations, in which the cascades were allowed to develop until completion. Further details on MD simulations is the topic of the next section.

5.2 Molecular dynamics

5.2.1 Basics

In *molecular dynamics* (MD), the time evolution for a system of atoms or other objects is studied by solving Newton's equations of motion numerically. This method has often been described jokingly as the physics of colliding billiard balls. The positions and velocities of the atoms are used for finding the positions and velocities after a short time step. An example of a possible simulation is shown in Fig. 8. As in BCA simulations (Section 5.1) and calculations of the nuclear stopping power (Section 4.1), the interatomic potential is vital to the performance and accuracy. The derivative of the potential gives the force on the atom, which is used in Newton's second law for determining the acceleration.

$$\mathbf{F} = -\frac{\mathrm{d}V(\mathbf{r})}{\mathrm{d}\mathbf{r}} \tag{14}$$

$$\mathbf{F} = m\mathbf{a} \tag{15}$$

The MD method is accurate only if the atoms move a short enough distance in one time step. Given typical velocities of atomic nuclei, the time step is limited to about one femtosecond (1×10^{-15} s). The short time step further limits the simulation time to nanoseconds at most, unless certain accelerating schemes are used [78, 79]. The *calculation* time of MD simulations can be made proportional to the number of atoms in the system. By dividing large simulation cells into smaller pieces that are distributed to separate computer cores, systems with over a 100 million atoms can be studied (see *e.g.* [80]). Further details about the principles of MD are found in [81].

To simulate bulk phenomena in simulation cells of nanometer size, periodic boundary conditions are applied. Caution must be exercised when using periodic boundary conditions in high energy cascade simulations, as not to create an unphysical situation in which a cascade overlaps with itself. If it is impractical to use a simulation cell that is large enough to contain the entire cascade, some kind of selective periodic boundary conditions can be an alternative, as is used in publication **IV**.

In simulations of cascade damage buildup, as in publications **I**-**III**, it is important to remove the excess energy added to the system by the recoils. In an experiment with a bulk sample, the heat from collision cascades is conducted to colder areas. The heat conduction can be introduced in MD simulations by applying temperature control to the boundary layers of the cell, given a collision cascade in the center of the cell. Berendsen temperature control [82] at boundaries is used in all simulations of recoils and inelastic thermal spikes in this thesis.

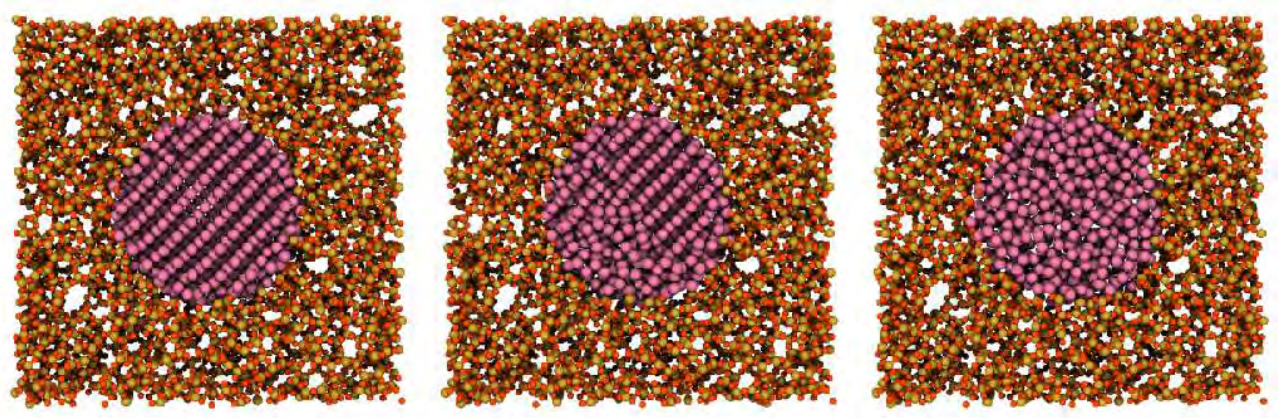

Figure 8: Cross-sectional snapshots from a molecular dynamics simulation of embedded Ge nanocrystal amorphization under ion irradiation. Damage accumulation is simulated by repeated 1 keV recoils in random locations in the cell. The amorphization dose is found to be much lower for nanocrystals than for bulk Ge.

Bonding and interaction between atoms is described by interatomic potentials, which approximate the general bonding trends by some relatively simple function of atom positions. In this work, we study materials with covalent bonds, such as SiC and SiO_2. To describe covalent materials, in which bonding is strongly directional, interatomic potentials with a bond angle dependence are frequently used. We use Stillinger-Weber potentials to describe Si-Si [83], Ge-Ge [84], and Si-Ge bonding and the Stillinger-Weber type potential by Watanabe [85, 86] for simulating amorphous SiO_2. We develop a Ge-O potential by scaling the SiO_2 potential to the properties of GeO_2. The Gao-Weber Tersoff potential for SiC [87] is used for the last part of this thesis.

All the MD simulations are carried out with the MD code PARCAS [88, 89, 90], which uses the fifth order Gear algorithm for integrating the equations of motion. PARCAS was developed by Nordlund *et al.* for simulations of cascades to be run in parallel by domain decomposition. PARCAS includes features like adaptive time step and electronic stopping that are essential in cascade simulations. They will be discussed in the following section.

5.2.2 MD for radiation effects

MD simulations display a number of features that make them suitable for studies of ion-solid interactions. The ballistic phase of collision cascades in solids only last about a picosecond (1×10^{-12} s), which is short enough to be modeled in full in MD. For longer time scale phenomena, like defect diffusion and clustering, it is common to use kinetic Monte Carlo (kMC) or other more approximate methods [9]. The length scale is also appropriate for exploring atomic level phenomena during ion irradiation. In addition, MD methods provide a sufficient level of accuracy for describing the

many-body effects that occur in a collision cascade. In the following, a few issues specific for MD simulations of ion irradiation are discussed.

In a simulation of ion irradiation, there is one or more atoms that have a higher than average velocity. For this reason, the time step needs to be shortened accordingly for the atom trajectories to remain correct and the energy to be conserved. Ion irradiation involves different time scales and it is often beneficial to adopt a variable time step that is short in the first, ballistic, stage of the cascade and increases as the atoms come to rest. The following adaptive time step selector [88] is used in PARCAS:

$$\Delta t_{\text{new}} = \min\left(\frac{k_t}{v}, \frac{E_t}{Fv}, 1.1\Delta t_{\text{old}}\right). \tag{16}$$

Here v is the maximum velocity in the system, which Δt is made inversely proportional to through the proportionality constant k_t. In strong collisions, the velocity will momentarily be low although the acceleration is high, hence the time step is made dependent on the maximum force F. E_t is a proportionality constant. The constraint $1.1\Delta t_{\text{old}}$ prevents the size of the time step from changing too drastically. In addition, there is a maximum possible time step that ensures a reasonable integration even if the atom velocities approach zero.

In strong collisions, the atom separation can be much shorter than would ever be possible under equilibrium conditions. Most interatomic potentials are fitted to equilibrium properties such as elastic constants, and they usually give a poor description, or can even be undefined, at very short ranges. Since the interatomic potential governs the scattering behavior in elastic collisions (Section 4.1), and therefore the nuclear stopping, it is of utmost importance in cascade simulations that the potential is accurate also at short distances. To achieve this, it is common to join the usual equilibrium potential to a more accurate repulsive short range potential at some distance that is shorter than the equilibrium atomic separation. The short range potential can be modeled in *ab initio* calculations [49], or one can use the ZBL universal repulsive potential (equation 10). The latter option was used in this work.

Even at projectile energies of a few tens of electronvolts, some energy is lost to electronic stopping, and this needs to be taken into account in cascade simulations. In the adiabatic or Born-Oppenheimer approximation, the velocity of electrons is assumed to be so much higher than that for the center of mass of the atom, that the electrons will adapt instantaneously (compared to timescales relevant to atomic motion) to movements of the nucleus and can be seen as constantly being in the ground state. The electronic energy loss is generally introduced in MD simulations as a frictional force on the moving atom. Analytical or empirical average stopping powers [43] as a function of the ion velocity serve as input, and gives acceptable accuracy in ion range calculations [91, 92].

The electronic damping force takes into account the transfer of energy from fast atoms to electrons, but we are neglecting that excess energy in the electronic system can diffuse and transport heat away from a collision cascade or transfer energy to the lattice through some electron-phonon coupling mechanism. The latter situation takes place in for instance swift heavy ion irradiation [93] or laser annealing [94]. The phenomenological models for such processes, in which the Born-Oppenheimer approximation is not valid, and their implementation in atomistic simulations is the topic of the following section.

5.3 Electronic energy deposition

Due to the complex nature of the structural changes caused by electronic excitations and ionization during ion irradiation, there are competing models for the interaction mechanism between the electronic system and the atomic lattice. There are several stages in the process that could be important [95, 96]. The passage of the ion causes ionization and excitation of electrons away from the ion trajectory, leading to a charge imbalance in the track area. Within a few femtoseconds, the space charges are neutralized and what remains is an area of excited electrons. Next, the electrons are assumed to thermalize, that is, adopt an electronic temperature, in a process that takes on the order of a few hundred femtoseconds. At this stage, the lattice atoms catch up and start adapting to the electronic system. Finally, there is interaction between the electrons and the lattice and excess energy in the electronic system is transferred to the lattice. When this coupled system reaches equilibrium, the systems relax and dissipate energy into the bulk of the material.

Different models for ion track formation focus on different stages during the course towards equilibrium. The Coulomb explosion model [97] suggests that the large charge imbalance right after the excitations leads to a violent discharge in the track area. Bringa *et al.* [98] have studied this model in MD simulations, but it might not be a realistic scenario based on the short range of Coulomb forces and the rapid charge redistribution by electrons [96]. In the bond weakening model and the exciton self-trapping model, the lattice modification is assumed to occur during the stage at which lattice atoms relax their positions in relation to the excited electronic system. In this work, materials modification by electronic stopping is described by the inelastic thermal spike model [99, 100], which is a phenomenological model that has been used quite extensively for studying swift heavy ion tracks [93], and agrees well with experimental observations [93, 101].

In the inelastic thermal spike model, the direct electron-lattice interaction is seen as the predominant mechanism of structural modification. The interaction is governed by the electron-phonon coupling strength g and the thermal conductivities K. The strength of the thermal spike model is its ability to make predictions through the so called two temperature model. We have two heat conduction

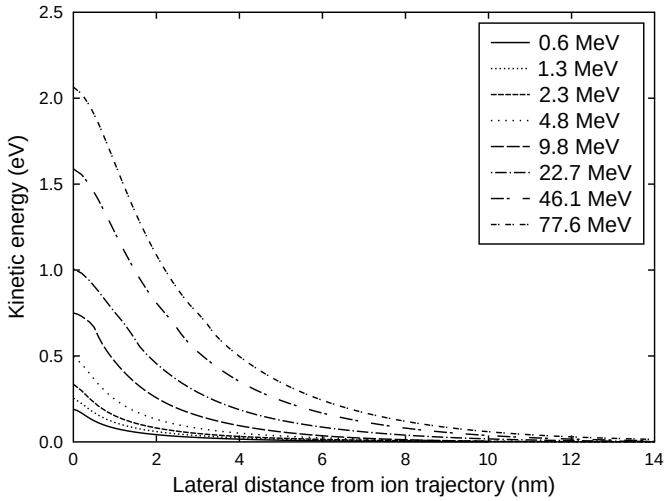

Figure 9: Inelastic thermal spike calculation of the heat in the lattice 100 fs after the start of electron-phonon equilibration. The calculations were carried out for gold ions in silica and used in MD simulations in publication **IV**.

equations, one for the lattice and one for the electronic system, and they are coupled through a term that is proportional to the difference in temperature T between the two systems.

$$C_e \frac{\delta T_e(r,t)}{\delta t} = \frac{1}{r}\frac{\delta}{\delta r}\left(rK_e \frac{\delta}{\delta r} T_e(r,t)\right) - g(T_e - T_a) + A(r,t) \quad (17)$$

$$C_a \frac{\delta T_a(r,t)}{\delta t} = \frac{1}{r}\frac{\delta}{\delta r}\left(rK_a \frac{\delta}{\delta r} T_a(r,t)\right) - g(T_e - T_a) \quad (18)$$

Here, the index e refers to the electrons and a to the atomic lattice. C is the specific heat and $A(r,t)$ is the initial distribution of energy in the electronic system due to the electronic stopping. Monte Carlo calculations for a heavy ion in water [102] provides an estimate for $A(r,t)$. In publications **III**-**VI**, the inelastic thermal spike model is used for estimating the heat transferred to the lattice due to electronic stopping during ion irradiation. According to the calculated electronic energy deposition profiles (Fig. 9), kinetic energy is given to the atoms in random directions to simulate an inelastic thermal spike.

Just in the last few years there has been significant interest and development in using *ab initio* calculations to model radiation damage [55, 56, 57, 58, 59]. Such simulations could alleviate the need for approximate models like the inelastic thermal spike and Coulomb explosion models or can give a physical foundation on which to base them. Using time dependent density functional theory (TDDFT), physicists have been able to explicitly study how electronic excitations are induced and even measure electronic stopping powers that are in good agreement with experimentally obtained values [55, 57].

Steps have also been taken to study the whole radiation problem [58, 59], including atomic motion, in what is called Ehrenfest dynamics. The currently available computational resources restrict the use of TDDFT methods to small exploratory cases as well as proofs of concept for the MD models.

5.4 Simulating high energy ion irradiation

There are different ways of modelling ion irradiation in MD simulations, a number of which have been used for the work in this thesis. The small cell size limits the ion energies at which the whole ion range and subcascades can be contained in the MD simulation to a few keV. It is therefore more common to study individual cascades due to primary knock-on atoms than to simulate the whole ion range.

The simplest alternative is simulating monoenergetic recoils, which is done in publications **I** and **II**. As shown in publication **II**, the amorphization rate of nanocrystals depends on the chosen recoil energy, which makes comparison with experiments difficult. A more realistic method is generating a recoil spectrum by for instance BCA or the MD-like code MDRANGE [88]. In publications **II** and **III**, the ion irradiation simulation is carried out by choosing random recoils according to the probabilities given by the recoil spectrum and the free flight path of the ion.

To study the precise collision dynamics along the ion path of MeV Au ions, it is sometimes beneficial to combine BCA and MD calculations [77], as is done in publication **IV**. BCA simulations are carried out for the ion and all subcascades down to 1 keV, which is well above the cut-off energy for validity of the binary collision approximation [103]. The recoil positions and velocities are used as input in the MD simulation, where the cascades evolve until completion. This method is illustrated in Fig. 10.

6 ION IRRADIATION OF EMBEDDED NANOCRYSTALS

Ion irradiation is an important tool in materials modification and analysis, and has been used extensively in research on nanoscale matter [13]. Especially the nuclear materials community is interested in the nanoscale, such as in ODS steels [20] and nanocrystalline SiC [104, 105]. Grain boundaries and other internal surfaces hinder the propagation of cascades and act as sinks for defects, which is why nanostructured materials may provide radiation tolerant materials for nuclear energy applications. Often, however, it is probable that the increased free energy in the system results in a lower amorphization dose, hence, studies are needed to determine the fundamental aspects of ion irradiation in nanostructures.

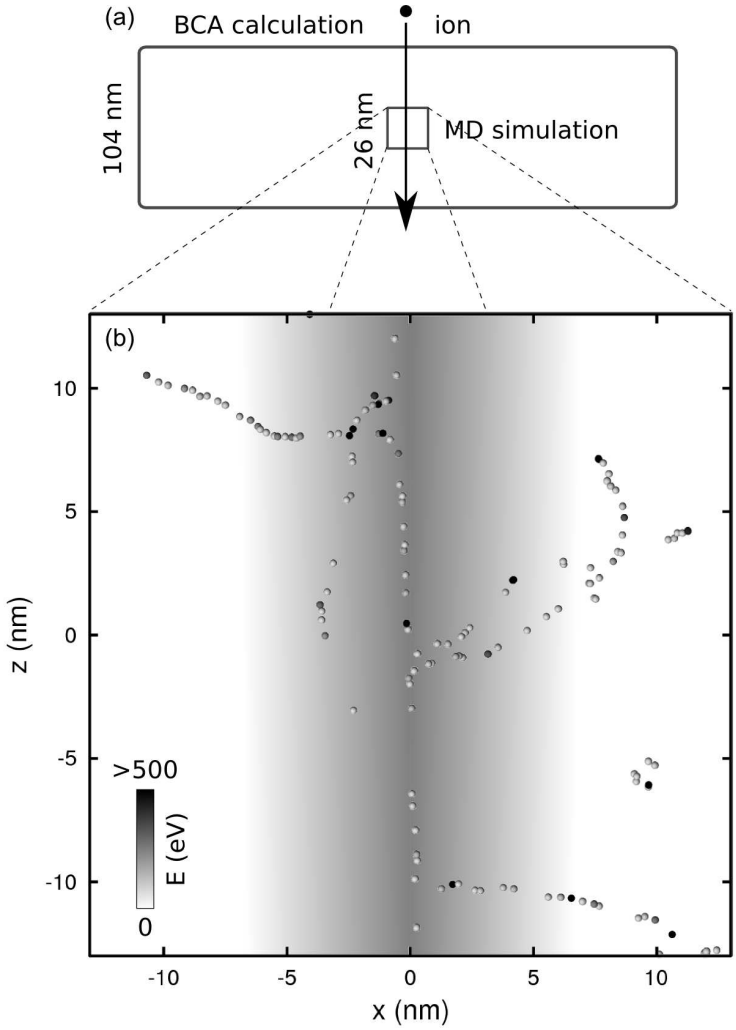

Figure 10: (a) Relation between BCA and MD in simulations of ion irradiation damage due to MeV ions. (b) Typical ion history of O and Si recoils along the path of 2.3 MeV Au ion in silica. The ion direction is in the negative *z* direction and the atoms are colored according to their kinetic energy as indicated by the legend. The shadowed area illustrates the thermal spike area.

Aside from the focus on tailoring and probing the properties of nanostructures, it is of fundamental interest for studying how radiation effects differ in nanomaterials compared to bulk materials. It was for instance found that Cu nanocrystals in silica below a certain size can become amorphous under ion irradiation [106], despite that bulk Cu, like many metals, do not amorphize under ion irradiation. In general, one can say that while numerous studies on irradiation effects in a plethora of different nanomaterials have been carried out (see e.g. references in [107, 13]), because of the many variables to control, the field is still developing and attempting to establish general trends.

6.1 Collision cascade damage in nanocrystals

Si or Ge nanocrystals in silica are fabricated by ion implantation of Si or Ge into silica and thermal annealing, whereupon segregation and formation of spherical crystallites is observed at the implantation depth [25, 108]. Ion beam methods are used for analyzing and modify surface properties, and it is hence interesting to investigate how embedded nanocrystals behave under ion irradiation. As an example, it was found experimentally that suitable ion irradiation can be used for modifying the size distribution of nanocrystal in a process called inverse Ostwald ripening [109, 110].

Collision cascade damage simulated by repeated monoenergetic 1 keV recoils makes 4 nm Ge nanocrystals in silica gradually lose their crystal structure over the course of tens of recoils. An atomistic illustration of a Ge nanocrystal is shown in Fig. 8. The nanocrystals are found to keep their spherical shape and the sharp interface between the two materials is kept relatively intact. For the most part, the phase transition from crystalline to amorphous starts at the nanocrystal-matrix interface, which acts as a seed for amorphization. Dissolution of nanocrystals into the matrix happens only for very small nanocrystals, but at irradiation doses higher than that for amorphization some dissolution is also noticed for larger sizes.

Fig. 11(a), from publication **II**, shows the amorphization under ion irradiation for Ge nanocrystals in silica and for bulk Ge as a function of the absorbed energy dose. The degree of disorder is measured by the deviation of the bond angles from that in the perfect crystal structure in the so called angular structure factor [111]. The nanocrystals reach full amorphization at a dose that is significantly lower than for the bulk, as would be expected from the initial state of disorder. Furthermore, there is a size dependent trend in the amorphization dose. This trend is even more clear if one compares the dose for reaching for instance 80 percent degree of amorphization. These results are supported by ion irradiation experiments analyzed by extended x-ray absorption spectroscopy (EXAFS) shown in Fig. 11(b). It is apparent from Fig. 11 that the initial degree of disorder depends on the nanocluster size, due to the larger surface-to-volume ratio for smaller spheres. The nanocluster-matrix interface also acts as a seed for amorphization, further promoting the loss of crystal structure upon defect formation.

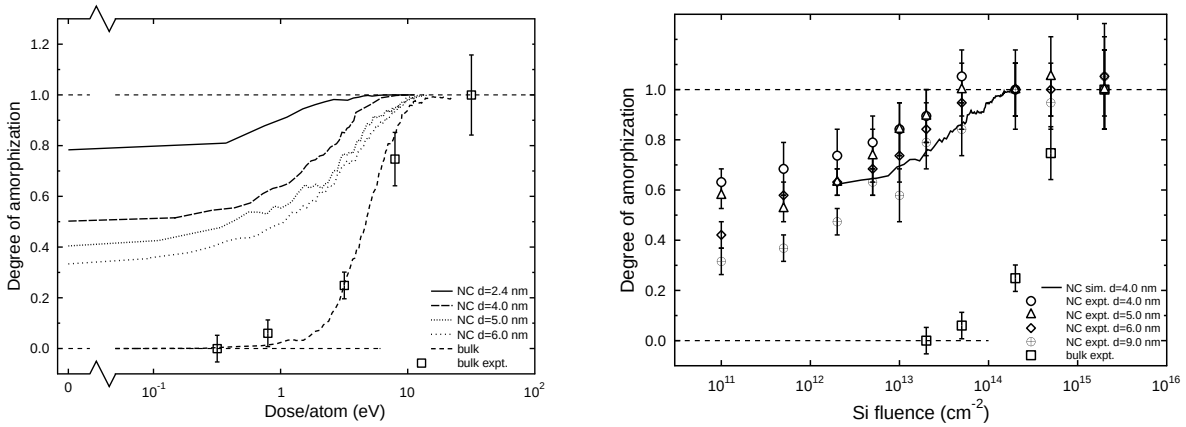

(a) (b)

Figure 11: Degree of amorphization for different sizes of Ge nanocrystals in silica under ion irradiation (a) simulated by 1 keV monoenergetic recoils and (b) studied in experiments by EXAFS Debye-Waller factor.

While direct quantitative comparison between experimental and simulation results is difficult, approximate calculations shows that the amorphization dose for the simulated nanocrystals seems to be slightly overestimated, as discussed in publication **II**. There are a couple of possible explanations for this discrepancy. One is the difference in structure and size of the nanocrystals. The simulations are carried out for one single size of nanocrystal, while the actual samples contain a distribution of sizes around some average. The nucleation and growth processes can also lead to inherent stress or defects in the embedded nanocrystals. Moreover, we speculate that the electronic stopping can have an effect on the cascade damage, which would not be seen in simulations of only collision cascades.

6.2 Electronic effects during ion irradiation of nanocrystals

As discussed in section 4.3, little is known about the interplay between electronic and nuclear stopping powers in ion irradiation damage. The electronic energy deposition by swift heavy ions is known to induce latent ion tracks in insulators, like silica. We speculated, and show in publication **III**, that electronic energy loss below the track production threshold can enhance cascade damage in Ge nanocrystals in silica. Irradiation by 1.8 MeV Si ions (S_n=0.054 keV/nm, S_e=1.65 keV/nm) and 3.6 MeV I ions (S_n=0.53 keV/nm, S_e=2.19 keV/nm) is studied in MD simulations with input from the inelastic thermal spike model for describing the local lattice heating due to the electronic energy loss.

Since the ion energies are too high to simulate in an MD simulation cell of practical size, we use the MDRANGE code [88] for calculating the primary recoil spectrum of the chosen ions. MDRANGE produces the same output as a BCA code, but in an MD framework which is sped up by only calculating

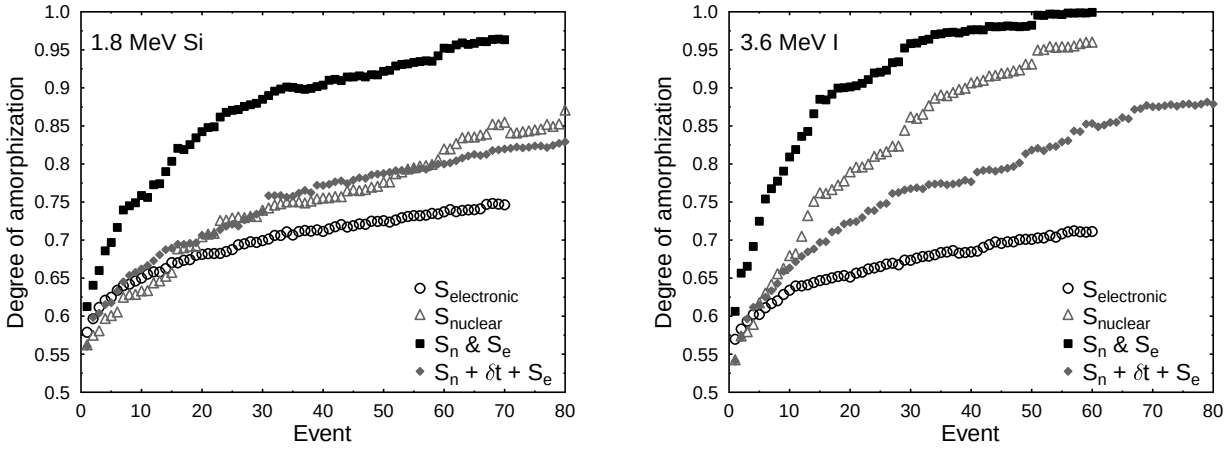

(a) (b)

Figure 12: Degree of amorphization of 4 nm Ge nanocrystals in silica as a function of the number of ion events for (a) 1.8 MeV Si and (b) 3.6 MeV I ions. To study the contribution of electronic stopping effects, simulations including only the inelastic thermal spike ($S_{electronic}$) or only the collision cascade ($S_{nuclear}$) are carried out. These are compared to simulation with simultaneous electronic and nuclear energy deposition (S_n & S_e) and nuclear and electronic energy deposition separated in time ($S_n + \delta t + S_e$).

ion-atom forces. The inelastic thermal spike calculations are carried out only for silica, for which it has been well tested and compared to experiments, so for this proof of concept, the silica energy deposition profiles (similar to those in Fig. 9) are used for the whole cell. The additional kinetic energy is added to each atom as velocity in a random direction.

In Fig. 12 it is demonstrated that the nanocrystals amorphize significantly faster if there is some heating due to electronic effects than if only collision cascades are simulated. Some degree of disorder is also created by the heating without the collision cascade. What is especially interesting is that the effect of the electronic energy deposition vanishes if there is a time separation between the collision cascade and the thermal spike. If the degree of disorder is analyzed both before and after each time-delayed thermal spike, it appears like the thermal spike anneals some of the damage caused by the collision cascades from 3.6 MeV I ions (Fig. 12 (b)), for which the nuclear stopping and therefore cascade damage is much more substantial than for the 1.8 MeV Si ions.

The electronic stopping powers for the two studied ions are similar in magnitude, but the nuclear stopping differs by one order of magnitude. This is manifested as a slower damage accumulation by the Si ions. It should be noted that the simulation method causes the effect of electronic heating to be exaggerated, since only direct hits to the nanocrystal are modeled. Realistically, a large part of the collision cascade damage would come from subcascades started away from the nanocrystal, in which case there would be no inelastic thermal spike.

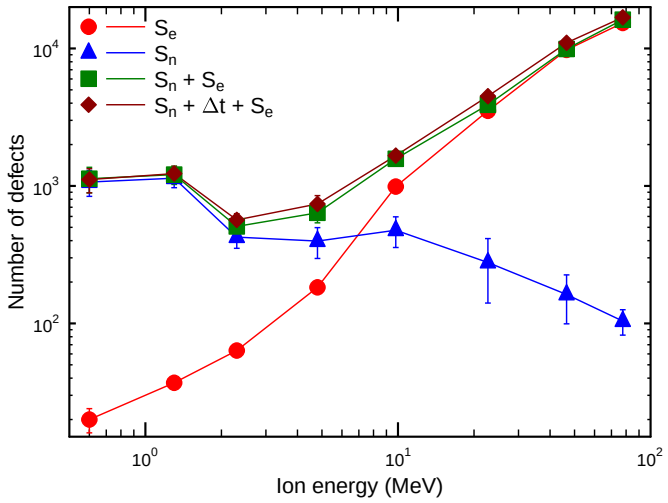

Figure 13: Number of defects in a silica MD simulation cell as a function of ion energy for electronic energy deposition (S_e), collision cascade (S_n), simultaneous inelastic thermal spike and cascade, as well as when the inelastic thermal spike is deposited 100 ps after the collision cascade.

7 COMBINED EFFECT OF NUCLEAR AND ELECTRONIC STOPPING POWERS IN BULK COMPOUNDS

The possible interaction effect between collision cascades and ion-electron interactions were discussed in section 4.3. It is clear from the previous section that the inelastic thermal spike from an ion can affect the collision cascades, but generalizing results in nanoclusters to bulk materials should be made only with great caution. In the following, molecular dynamics simulations describing the combined effect of collision cascade damage and inelastic thermal spikes in bulk materials are presented.

7.1 Synergy between electronic and nuclear stopping in silica

Heavy ions have high nuclear stopping at low kinetic energies and high electronic stopping at high energies. We set out to study the irradiation damage in the intermediate region where the stopping power crosses over from nuclear stopping to electronic stopping and the two stopping powers are of similar magnitude. Toulemonde *et al.* [66] studied Au irradiation of silica in the ion energy range 0.3-185 MeV, in which the nuclear stopping decreases from 3.2 to 0.16 keV/nm while the electronic stopping increases from 0.26 to 16.2 keV/nm (Fig. 4). The threshold for continuous track formation is smaller than 4 keV/nm [93], but Toulemonde *et al.* found that the electronic stopping contributes to irradiation damage also below this energy. MD simulations of this phenomenon can shed light on the interaction mechanism between nuclear and electronic stopping.

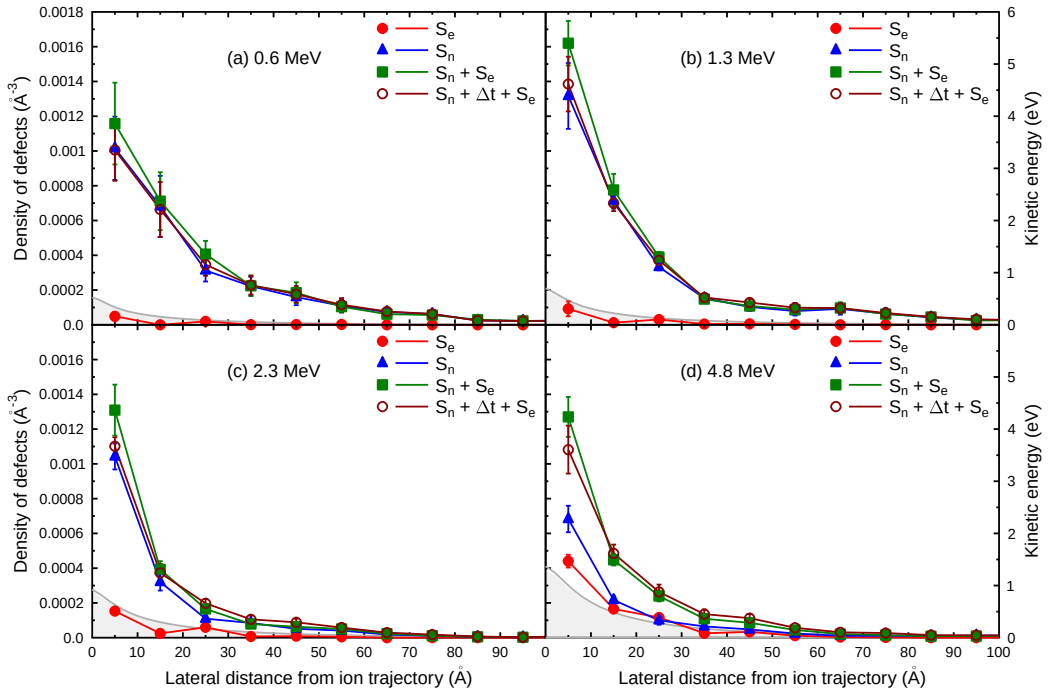

Figure 14: Defect density as a function of lateral distance from the ion path for different Au ion energies in silica. The gray shaded area (right-hand y-axis) represents the electronic energy deposition.

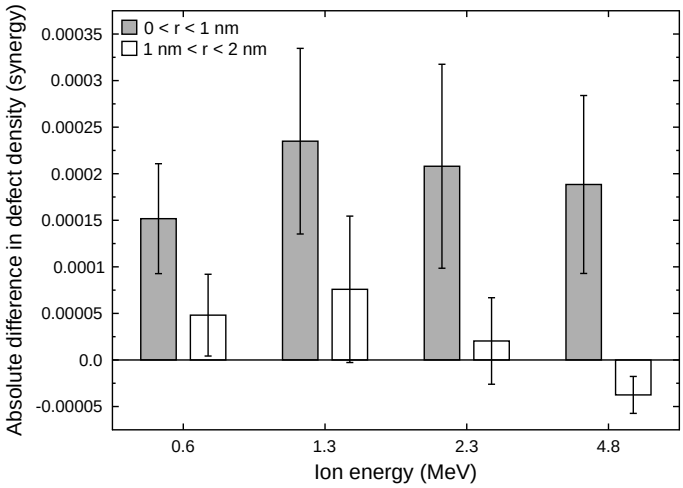

Figure 15: Difference in density of defects in the area close to the ion trajectory between simultaneous and sequential nuclear and electronic energy deposition (see Fig. 14).

To make MD simulations possible, the electronic excitations are assumed to only affect the lattice in the form of local heating due to electron-phonon coupling. Consequently, the inelastic thermal spike model (section 5.3) is used for calculating the temperature in the lattice as a function of time and distance from the ion trajectory. The coordination defects in a simulation cell are analyzed after i) thermal spike, ii) collision cascade, iii) simultaneous collision cascade and thermal spike, and iv) sequential deposition of collision cascade and thermal spike with a 100 ps delay. Fig. 13 demonstrates that both damage mechanisms contribute to damage in the intermediate energy regime.

In Fig. 14 the defect densities are plotted as a function of the distance from the ion path. This can make the contribution from the electronic stopping more clear, since the electronic energy deposition also varies with lateral distance from the ion. We find that the thermal spike contributes most to the damage in the area closest to the ion trajectory, which is expected since the instantaneous temperature in the thermal spike is lower the further away from the ion. What is less obvious is that the results, presented in publication **IV**, suggest that there is a nonlinear synergy between the collision cascade and electronic heating in the core of the ion track. The effect is more evident in Fig. 15, in which the difference between the defects due to simultaneous and sequential deposition of the nuclear and electronic stopping is plotted.

7.2 Swift heavy ion-induced defect recovery in ion irradiated silicon carbide

In semiconductors, which have a smaller band gap than insulators, the effect of intense electronic excitations is less severe than in insulators like silica. For instance in SiC, ion tracks have not yet been observed, but recent experimental studies of swift heavy ion irradiation in previously irradiation damaged SiC [67, 68] suggest that the high electronic stopping power leads to recovery of damage. It was conjectured that local heating along the ion trajectory can explain this observation.

As a proof of concept, we simulate a thermal spike from an 870 MeV Pb ion in a SiC cell with a high Frenkel pair concentration. Fig. 16 shows the remaining vacancies and interstitials after the electronic energy deposition and relaxation. In the core of the track there is melting and some damage creation by the local heating, but outside the core there is significant defect recovery extending out to almost 10 nm from the ion trajectory. This large cross section for recovery indicates that recrystallization of a sample can be achieved by reasonable ion fluences.

Molecular dynamics simulations of 870 MeV Pb ion irradiation in a buried layer in SiC that is either amorphous (Fig. 17 (a)) or partially disordered (Fig. 17 (b)) reveal significant recrystallization. An atomistic illustration showing the sharpening of the interface in the amorphous layer is found in Fig.

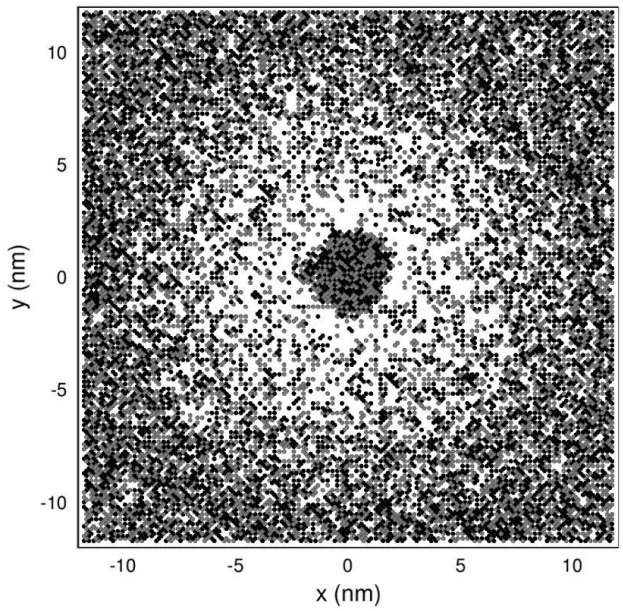

Figure 16: Vacancies (gray) and interstitials (black) after one inelastic thermal spike in a 10 nm thick layer of a SiC MD simulation cell with an initially uniform concentration of defects. The inelastic thermal spike corresponds to the deposition of energy to the electrons from an 870 MeV Pb ion.

18. In the fully amorphous layer, recrystallization takes place at the amorphous-to-crystalline interface, where there are crystalline seeds. In the partially disordered layer, such remaining crystallinity is present throughout the layer, and consequently recovery is observed over the whole damage thickness. Moreover, the damage level decreases with increasing ion fluence, as evidenced by experiments as well as simulations of multiple thermal spike overlaps.

There is excellent qualitative agreement between the simulations and Rutherford backscattering spectrometry (RBS) analysis of irradiated samples, as we can see in publication **V**. Fig. 19 shows high-resolution cross-sectional transmission electron microscopy (X-HRTEM) images and corresponding fast-Fourier transform (FFT) of the partially amorphous sample before and after 870 MeV Pb irradiation. The RBS analysis and simulation results are confirmed by the decrease in the extent of disordered areas and the sharpening of the peaks in the FFT. The fact that the thermal spike simulations reproduce experimental results from swift heavy ion irradiation implies that electron-phonon coupling is the predominant recovery mechanism in SiC.

8 CONCLUSIONS

Understanding the mechanisms of damage and structural modification in materials due to ion irradiation is important both for mitigating destructive effects in a radiative environment and for the

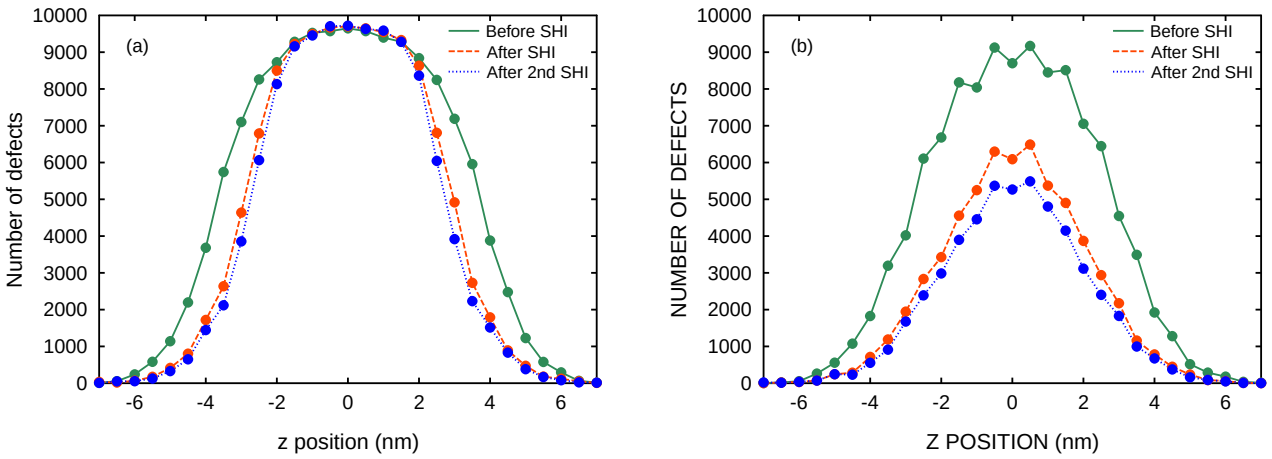

Figure 17: Swift heavy ion-induced recovery in (a) an amorphous and (b) a partially disordered layer in SiC simulated with MD. The effect of the swift heavy ion is simulated as an inelastic thermal spike. In the amorphous layer recrystallization takes place at the amorphous to crystalline interface. In the partially disordered layer there is recovery over the whole damaged layer.

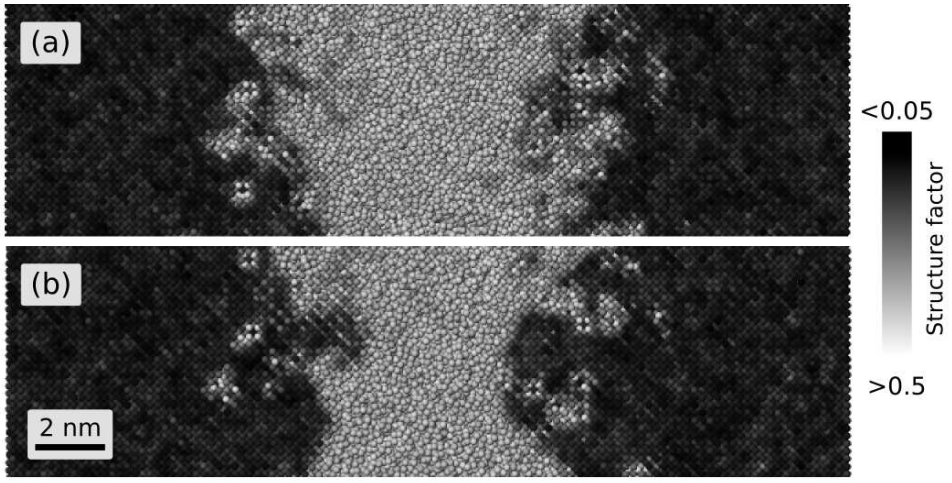

Figure 18: Section of the amorphous layer in SiC before and after the inelastic thermal spike from a swift heavy ion. The atoms are colored according to their angular structure factor.

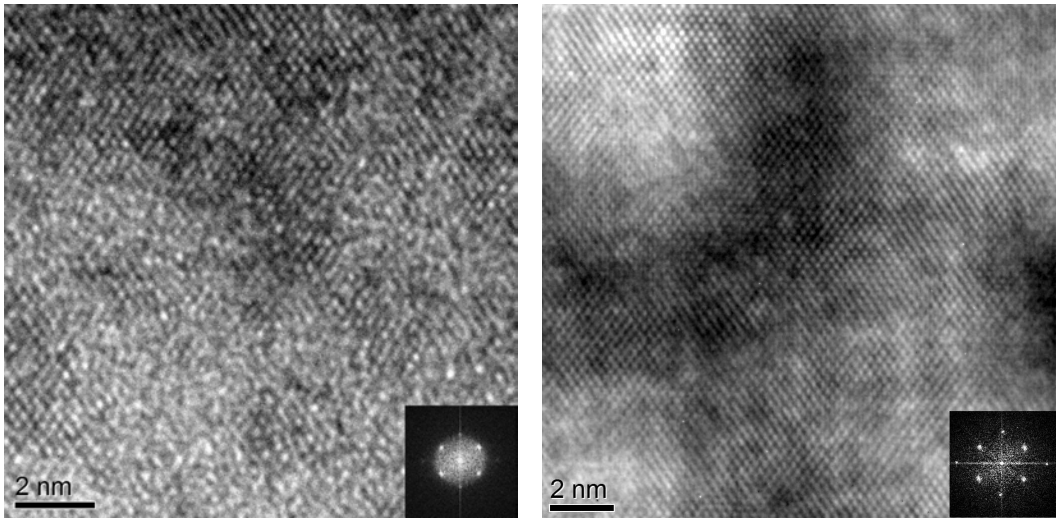

(a)

Figure 19: High-resolution TEM micrograph and FFT of single crystalline SiC sample after (a) 100 keV Fe irradiation and (b) 100 keV Fe irradiation followed by 870 MeV Pb irradiation. During the second irradiation step, the high electronic energy loss of the ions induces recrystallization of the damage created in the first irradiation step.

controlled use of ion beams in industry and research. Displacement cascades in single crystalline or amorphous materials are fairly well understood, but there are many open questions regarding irradiation effects in more complex materials, like nanocomposites, or at moderate to high electronic energy losses. For describing such complicated phenomena, we need collaborative efforts by experimental and computational scientists.

In this thesis, it was shown in molecular dynamics simulations that Si and Ge nanocrystals in silica amorphize under ion irradiation, and that the amorphization dose is size dependent. The initial state of partial disorder, as well as the interface of the nanocrystals that act as a seed for amorphization, both ensure that the nanocrystals lose their crystal structure much easier than the bulk. These results supported experimental measurements of the change in Debye-Waller factor as a function of ion fluence for samples containing nanocrystals. The discrepancy in the absolute dose of amorphization inspired an investigation of the role of electronic effects in ion irradiation damage. Indeed, we found that the presence of an inelastic thermal spike leads to a significantly lower amorphization dose.

A systematic investigation of the nuclear and electronic stopping damage mechanisms in silica was carried out using molecular dynamics simulations with input from the inelastic thermal spike model that describes the lattice heating due to electronic excitations. It was found that electronic excitations produce damage also at moderate ion energies, and this damage contributes to the collision cascade damage. There were indications of a synergy between the two damage mechanisms, but further studies are needed to confirm this effect.

In silicon carbide, on the other hand, it was experimentally observed that swift heavy ions can produce defect recovery of ion irradiation damaged samples. It was speculated that local heating due to the electronic excitations could be responsible. Molecular dynamics simulations carried out in this work confirmed this observation and found indications of a very large recovery cross-section. Because of the excellent agreement between the experiments and simulations, we concluded that the observed recovery can be explained in the inelastic thermal spike framework.

In conclusion, the work in this thesis demonstrates that there is an intricate relationship between electronic and nuclear stopping in ion-solid interactions. Specifically, electronic energy deposition can both create and anneal structural damage. With results in good agreement with experiments, computer simulations proves a valuable tool to disassemble even very complex phenomena and further the understanding of them.

ACKNOWLEDGMENTS

I wish to thank the head of the Department of Physics at the University of Helsinki, Prof. Juhani Keinonen, as well as the head of the Accelerator Laboratory, Prof. Jyrki Räisänen, for providing the facilities for the research presented in this thesis. Financial support from Svenska kulturfonden and Waldemar von Frenckells stiftelse is gratefully acknowledged.

I have had the fortune of working with a group of very dedicated supervisors and accomplished scientists. Many warm thanks are due to Dr. Flyura Djurabekova and Prof. Kai Nordlund for introducing me to the research field as well as to computational methods and for always giving me their full support. Their optimism and enthusiasm is truly contagious. I also wish to thank Dr. Olli Pakarinen for, through his thoroughness and persistence, being a great role model for an aspiring scientist. I am most grateful to Prof. Bill Weber and Prof. Yanwen Zhang for welcoming me into their research group at University of Tennessee, Knoxville and for guiding my work forward and sharing with me some of their enormous expertise in ion irradiation effects.

This work would not have been possible without the help of many scientific collaborators across the world. Special thanks are due to Dr. Marcel Toulemonde, Dr. Leandro Araujo, Prof. Mark Ridgway, and Dr. Aurélien Debelle.

I thank my colleagues, past and present, at the Accelerator Laboratory in Helsinki for creating such a unique atmosphere and sense of community. My warm thanks also to my colleagues and friends in Knoxville, who made me feel at home very far away from home.

I am grateful for having such incredible support from my family and friends. Most importantly, I would like to thank my husband Niklas for his love and encouragement throughout this journey.

Helsinki, November 12, 2012
Marie Backman

References

1. H. Geiger and E. Marsden, *On a Diffuse Reflection of the α-Particles*, Proc. Roy. Soc. A **82**, 495 (1909).

2. E. Rutherford, *The Scattering of α and β Particles by Matter and the Structure of the Atoms*, Philos. Mag. **21**, 669 (1911).

3. N. Bohr, *On the Constitution of Atoms and Molecules*, Philos. Mag. **26**, 1 (1913).

4. N. Bohr, *On the Theory of Decrease of Velocity of Moving Electrified Particles on Passing through Matter*, Philos. Mag. Series 6 **25**, 10 (1913).

5. N. Bohr, *On the decrease of velocity of swiftly moving electrified particles in passing through matter*, Philos. Mag. **30**, 581 (1915).

6. N. Bohr, *The penetration of atomic particles through matter*, Mat. Fys. Medd. Dan. Vid. Selsk. **18**, 1 (1948).

7. L. Rubin and J. Poate, *Ion Implantation in Silicon Technology*, Indus. Physicist **9**, 12 (2003).

8. L. Pavesi, L. D. Negro, C. Mazzoleni, G. Franzò, and F. Priolo, *Optical gain in silicon nanocrystals*, Nature **408**, 440 (2000).

9. G. S. Was, in *Fundamentals of Radiation Materials Science* (Springer, Berlin Heidelberg, 2007).

10. V. K. Alimov and J. Roth, *Hydrogen isotope retention in plasma-facing materials: review of recent experimental results*, Phys. Scr. **T128**, 6 (2007).

11. U. Amaldi and G. Kraft, *Radiotherapy with beams of carbon ions*, Rep. Prog. Phys. **68**, 1861 (2005).

12. M. Durante and J. S. Loeffler, *Charged particles in radiation oncology*, Nat. Rev. Clin. Oncol. **7**, 37 (2010).

13. A. V. Krasheninnikov and K. Nordlund, *Ion and electron irradiation-induced effects in nanostructured materials*, J. Appl. Phys. **107**, 071301 (2010).

14. R. Erni and N. D. Browning, *Quantification of the size-dependent energy gap of individual CdSe quantum dots by valence electron energy-loss spectroscpy*, Ultramicroscopy **107**, 267 (2007).

15. S. Zhang, D. Sun, Y. Fu, and H. Du, *Recent advances of superhard nanocomposite coatings: a review*, Surf. Coat. Technol. **167**, 113 (2003).

16. J. Musil, F. Regent, Z. Soukup, J. Vicek, and J. G. Han, *Recent progress in hard nanocomposite coatings*, High Temp. Mater. Processes (New York) **4**, 553 (2000).

17. in *Nanocomposite thin films and coatings*, edited by S. Zhang and N. Ali (Imperial College Press, London, 2007), Chap. 5. Properties of hard nanocomposite thin films.

18. S. Zhang, D. Sun, Y. Fu, and H. Du, *Toughening of hard nanostructural thin films: a critical review*, Surf. Coat. Technol. **198**, 2 (2005).

19. G. R. Odette, M. J. Alinger, and B. D. Wirth, *Recent Developments in Irradiation-Resistant Steels*, Annu. Rev. Mater. Res. **38**, 471 (2008).

20. A. Hirata, T. Fujita, Y. R. Wen, J. H. Schneibel, C. T. Liu, and M. W. Chen, *Atomic structure of nanoclusters in oxide-dispersion-strengthened steels*, Nature Mater. **10**, 922 (2011).

21. I. Freestone, N. Meeks, M. Sax, and C. Higgitt, *The Lycurgus Cup – A Roman Nanotechnology*, Gold Bulletin **40**, 270 (2007).

22. A. P. Alivisatos, *Semiconductor Clusters, Nanocrystals, and Quantum Dots*, Science **271**, 933 (1996).

23. S. Eustis and M. A. El-Sayed, *Why gold nanoparticles are more precious than pretty gold: Noble metal surface plasmon resonance and its enhancement of the radiative and nonradiative properties of nanocrystals of different shapes*, Chem. Soc. Rev. **35**, 209 (2005).

24. L. T. Canham, *Silicon quantum wire array fabrication by electrochemical and chemical dissolution of wafers*, J. Appl. Phys. **57**, 1046 (1990).

25. T. Shimizu-Iwayama, M. Ohshima, T. Niimi, S. Nakao, K. Saitoh, T. Fujita, and N. Itoh, *Visible photoluminescence related to Si precipitates in Si^+-implanted SiO_2*, J. Phys.: Condens. Matter **5**, L375 (1993).

26. S. Godefroo, M. Hayne, M. Jivanescu, A. Stesmans, M. Zacharias, O. I. Lebedev, G. Van Tendeloo, and V. V. Moshchalkov, *Classification and control of the origin of photoluminescence from Si nanocrystals*, Nature Nanotechnol. **3**, 174 (2008).

27. D. C. Hannah, J. Wang, P. Podsiadlo, M. K. Y. Chan, A. Demortière, D. J. Gosztola, V. B. Prakapenka, G. C. Schatz, U. Kortshagen, and R. D. Schaller, *On the Origin of Photoluminescence in Silicon Nanocrystals: Pressure-Dependent Structural and Optical Studies*, Nano Lett. **12**, 4200 (2012).

28. S. Tiwari, F. Rana, H. Hanafi, A. Harstein, E. F. Crabbé, and K. Chan, *A silicon nanocrystals based memory*, Appl. Phys. Lett. **68**, 1377 (1996).

29. A. Martínez, J. Blasco, P. Sanchis, J. V. Galán, J. García-Rupérez, E. Jordana, P. Gautier, Y. Lebour, S. Hernández, R. Spano, R. Guider, N. Daldosso, B. Garrido, J. M. Fedeli, L. Pavesi, and J. Martí, *Ultrafast All-Optical Switching in a Silicon-Nanocrystal-Based Silicon Slot Waveguide at Telecom Wavelengths*, Nano Letters **10**, 1506 (2010).

30. E.-C. Cho, S. Park, X. Hao, D. Song, G. Conibeer, S.-C. Park, and M. A. Green, *Silicon quantum dot/crystalline silicon solar cells*, Nanotechnology **19**, 245201 (2008).

31. R. J. Walters, P. G. Kik, J. D. Casperson, and H. A. Atwater, *Silicon optical nanocrystal memory*, Appl. Phys. Lett. **85**, 2622 (2004).

32. R. J. Walters, G. I. Bourianoff, and H. A. Atwater, *Field-effect electroluminescence in silicon nanocrystals*, Nature Mater. **4**, 143 (2005).

33. G. Cao, *Nanostructures & Nanomaterials: Synthesis, Properties & Applications* (Imperial College Press, London, 2004).

34. T.-C. Chang, F.-Y. Jian, S.-C. Chen, and Y.-T. Tsai, *Developments in nanocrystal memory*, Mater. Today **14**, 608 (2011).

35. L. C. Kimerling, *Silicon microphotonics*, Appl. Surf. Sci. **159-160**, 8 (2000).

36. J. R. Rodríguez Núñez and J. G. C. Veinot, *Commentary: Silicon nanocrystals and their role in photonics*, J. Nanophotonics **6**, 060302 (2012).

37. J. De Blauwe, *Nanocrystal Nonvolatile Memory Devices*, IEEE Trans. Nanotechnol. **1**, 72 (2002).

38. P. A. Packan, *Pushing the Limits*, Science **285**, 2079 (1999).

39. J. J. Welser, S. Tiwari, S. Rishton, K. Y. Lee, and Y. Lee, *Room temperature operation of quantum-dot flash memory*, IEEE Electron Device Lett. **18**, 278 (1997).

40. R. Muralidhar *et al.*, *An embedded silicon nanocrystal nonvolatile memory for the 90nm technology node operating at 6V*, IEEE ICICDT 31 (2004).

41. G. Chindalore, J. Yater, H. Gasquet, M. Suhail, S.-T. Kang, C. M. Hong, N. Ellis, G. Rinkenberger, J. Shen, M. Herrick, W. Malloch, R. Syzdek, K. Baker, and K.-M. Chang, *Embedded split-gate flash memory with silicon nanocrystals for 90nm and beyond*, IEEE VLSI Tech. 136 (2008).

42. C. Gerardi, G. Molas, G. Albini, E. Tripiciano, M. Gely, A. Emmi, O. Fiore, E. Nowak, D. Mello, M. Vecchio, L. Masarotto, R. Porthogese, B. De Salvo, S. Deleonibus, and A. Maurelli, *Performance and reliability of a 4Mb Si nanocrystal NOR Flash memory with optimized 1T memory cells*, IEEE IEDM 1 (2008).

43. J. F. Ziegler, J. P. Biersack, and U. Littmark, *The stopping and range of ions in solids* (Pergamon, New York, 1985).

44. M. Nastasi, J. W. Mayer, and J. K. Hirvonen, *Ion-Solid Interactions* (Cambridge University Press, Cambridge, 1996).

45. P. Sigmund, *Particle Penetration and Radiation Effects* (Springer, Berlin, 2006).

46. P. Sigmund, *Stopping power: Wrong terminology*, ICRU News 5 (2000).

47. J. F. Ziegler, SRIM-2008 software package, available online at *http://www.srim.org*.

48. W.-K. Chu, J. W. Mayer, and M.-A. Nicolet, *Backscattering Spectrometry* (Academic Press, London, 1978).

49. K. Nordlund, N. Runeberg, and D. Sundholm, *Repulsive interatomic potentials calculated using Hartree-Fock and density-functional methods*, Nucl. Instrum. Meth. Phys. Res. B **132**, 45 (1997).

50. R. M. Martin, *Electronic Structure: Basic Theory and Practical Methods* (Cambridge University Press, Cambridge, 2008).

51. R. S. Averback and T. Diaz de la Rubia, in *Solid State Physics*, edited by H. Ehrenfest and F. Spaepen (Academic Press, New York, 1998), Vol. 51, pp. 281–402.

52. Adapted from the Wikimedia Commons file "File:Heatspikecollisioncascade.png" *http://commons.wikimedia.org/wiki/File:Heatspikecollisioncascade.png*.

53. H. Bethe, *Zur Theorie des Durchgangs schneller Korpuskularstrahlen durch Materie*, Ann. Physik **397**, 325 (1930).

54. P. Sigmund, *Reciprocity in the electronic stopping of slow ions in matter*, Eur. Phys. J. D **47**, 45 (2008).

55. R. Hatcher, M. Beck, A. Tackett, and S. T. Pantelides, *Dynamical Effects in the Interaction of Ion Beams with Solids*, Phys. Rev. Lett. **100**, 103201 (2008).

56. C. P. Race, D. R. Mason, M. W. Finnis, W. M. C. Foulkes, A. P. Horsfield, and A. P. Sutton, *The treatment of electronic excitations in atomistic models of radiation damage in metals*, Rep. Prog. Phys. **73**, 116501 (2010).

57. M. Ahsan Zeb, J. Kohanoff, D. Sánchez-Portal, A. Arnau, J. J. Juaristi, and E. Artacho, *Electronic Stopping Power in Gold: The Role of d Electrons and the H/He Anomaly*, Phys. Rev. Lett. **108**, 225504 (2012).

58. A. A. Correa, J. Kohanoff, E. Artacho, D. Sánchez-Portal, and A. Caro, *Nonadiabatic Forces in Ion-Solid Interactions: The Initial Stages of Radiation Damage*, Phys. Rev. Lett. **108**, 213201 (2012).

59. S. Bubin, B. Wang, S. Pantelides, and K. Varga, *Simulation of high-energy ion collisions with graphene fragments*, Phys. Rev. B **85**, 235435 (2012).

60. H. M. Presby and W. L. Brown, *Refractive index variations in proton-bombarded fused silica*, Appl. Phys. Lett. **24**, 511 (1974).

61. E. P. EerNisse and C. B. Norris, *Introduction rates and annealing of defects in ion-implanted SiO_2 layers on Si*, J. Appl. Phys. **45**, 5196 (1974).

62. S. Nagata, H. Katsui, B. Tsuchiya, A. Inouye, S. Yamamoto, K. Toh, and T. Shikma, *Damage process and luminescent characteristics in silica glasses under ion irradiation*, J. Nucl. Mater. **386-388**, 1045 (2009).

63. A. Iwase, S. Sasaki, T. Iwata, and T. Nihira, *Anomalous Reduction of Stage-I Recovery in Nickel Irradiated with Heavy Ions in the Energy Range 100-120 MeV*, Phys. Rev. Lett. **58**, 2450 (1987).

64. A. Dunlop, D. Lesueur, J. Morillo, J. Dural, R. Spohr, and J. Vetter, *High electronic excitations and damage production in GeV-ion-irradiated metals*, Nucl. Instrum. Meth. Phys. Res. B **48**, 419 (1990).

65. F. Jaque and P. D. Townsend, *Luminescence during ion implantation of silica*, Nucl. Instrum. Meth. **182/183**, 781 (1981).

66. M. Toulemonde, W. J. Weber, G. Li, V. Shutthanandan, P. Kluth, T. Yang, Y. Wang, and Y. Zhang, *Synergy of nuclear and electronic energy losses in ion-irradiation processes: The case of vitreous silicon dioxide*, Phys. Rev. B **83**, 054106 (2011).

67. A. Benyagoub, A. Audren, L. Thomé, and F. Garrido, *Athermal crystallization induced by electronic excitations in ion-irradiated silicon carbide*, Appl. Phys. Lett. **89**, 241914 (2006).

68. A. Audren, I. Monnet, D. Gosset, Y. Leconte, X. Portier, L. Thomé, F. Garrido, A. Benyagoub, M. Levalois, N. Herlin-Boime, and C. Reynaud, *Effects of electronic and nuclear interactions in SiC*, Nucl. Instrum. Meth. Phys. Res. B **267**, 976 (2009).

69. A. Kamarou, W. Wesch, E. Wendler, and S. Klaumünzer, *Damage formation and annealing in InP due to swift heavy ions*, Nucl. Instrum. Meth. Phys. Res. B **225**, 129 (2004).

70. M. T. Robinson and O. S. Oen, *Computer Studies of the Slowing Down of Energetic Atoms in Crystals*, Phys. Rev. **132**, 2385 (1963).

71. J. F. Ziegler, *SRIM-2003*, Nucl. Instrum. Meth. Phys. Res. B **219**, 1027 (2004).

72. B. D. Wirth, K. Nordlund, D. G. Whyte, and D. Xu, *Fusion materials modeling: Challenges and opportunities*, MRS Bulletin **36**, 216 (2011).

73. S. Agostinelli *et al.*, GEANT4 – *a simulation toolkit*, Nucl. Instrum. Meth. Phys. Res. A **506**, 250 (2003).

74. O. S. Oen, D. K. Holmes, and M. T. Robinson, *Ranges of Energetic Atoms in Solids*, J. Appl. Phys. **34**, 302 (1963).

75. J. P. Biersack and L. G. Haggmark, *A Monte Carlo computer program for the transport of energetic ions in amorphous targets*, Nucl. Instrum. Meth. **174**, 257 (1980).

76. T. S. Pugacheva, F. G. Jurabekova, Y. Miyagawa, and S. K. Valiev, *Computer simulation of SiC and B_4C sputtering by Ar^+ and He^+ ions bombardment*, Nucl. Instrum. Meth. Phys. Res. B **127/128**, 260 (1997).

77. M. Posselt, *Prediction of the morphology of the as-implanted damage in silicon using a novel combination of BCA and MD simulations*, Mater. Sci. Semicond. Process. **3**, 317 (2000).

78. A. F. Voter, *Parallel replica method for dynamics of infrequent events*, Phys. Rev. B **57**, R13985 (1998).

79. M. R. Sørensen and A. F. Voter, *Temperature-accelerated dynamics for simulation of infrequent events*, J. Chem. Phys. **112**, 9599 (2000).

80. J. Samela and K. Nordlund, *Atomistic simulation of the transition from atomistic to macroscopic cratering*, Phys. Rev. Lett. **101**, 027601 (2008).

81. M. P. Allen and D. J. Tildesley, *Computer Simulation of Liquids* (Oxford University Press, Oxford, 1987).

82. H. J. C. Berendsen, J. P. M. Postma, W. F. van Gunsteren, A. DiNola, and J. R. Haak, *Molecular dynamics with coupling to an external bath*, J. Chem. Phys. **81**, (1984).

83. F. H. Stillinger and T. A. Weber, *Computer simulation of local order in condensed phases of silicon*, Phys. Rev. B **31**, 5262 (1985).

84. K. Ding and H. C. Andersen, *Molecular-dynamics simulation of amorphous germanium*, Phys. Rev. B **34**, 6987 (1986).

85. T. Watanabe, D. Yamasaki, K. Tatsumura, and I. Ohdomari, *Improved interatomic potential for stressed Si, O mixed systems*, Appl. Surf. Sci. **234**, 207 (2004).

86. J. Samela, K. Nordlund, V. N. Popok, and E. E. B. Campbell, *Origin of complex impact craters on native oxide coated silicon surfaces*, Phys. Rev. B **77**, 075309 (2008).

87. F. Gao and W. J. Weber, *Empirical potential approach for defect properties in 3C-SiC*, Nucl. Instrum. Meth. Phys. Res. B **191**, 504 (2002).

88. K. Nordlund, *Molecular dynamics simulation of ion ranges in the 1 – 100 keV energy range*, Comput. Mater. Sci. **3**, 448 (1995).

89. K. Nordlund, M. Ghaly, R. S. Averback, M. Caturla, T. Diaz de la Rubia, and J. Tarus, *Defect production in collision cascades in elemental semiconductors and FCC metals*, Phys. Rev. B **57**, 7556 (1998).

90. M. Ghaly, K. Nordlund, and R. S. Averback, *Molecular dynamics investigations of surface damage produced by keV self-bombardment of solids*, Phil. Mag. A **79**, 795 (1999).

91. J. Sillanpää, K. Nordlund, and J. Keinonen, *Electronic stopping of Si from a three-dimensional charge distribution*, Phys. Rev. B **62**, 3109 (2000).

92. J. le Page, D. R. Mason, C. P. Race, and W. M. C. Foulkes, *How good is damped molecular dynamics as a method to simulate radiation damage in metals?*, New J. Phys. **11**, 013004 (2009).

93. P. Kluth, C. S. Schnohr, O. H. Pakarinen, F. Djurabekova, D. J. Sprouster, R. Giulian, M. C. Ridgway, A. P. Byrne, C. Trautmann, D. J. Cookson, K. Nordlund, and M. Toulemonde, *Fine Structure in Swift Heavy Ion Tracks in Amorphous SiO_2*, Phys. Rev. Lett. **101**, 175503 (2008).

94. D. Bouilly, D. Perez, and L. J. Lewis, *Damage in materials following ablation by ultrashort laser pulses: A molecular-dynamics study*, Phys. Rev. B **76**, 184119 (2007).

95. N. Itoh and A. M. Stoneham, *Materials Modification by Electronic Excitation* (Cambridge University Press, Cambridge, 2001).

96. N. Itoh, D. M. Duffy, S. Khakshouri, and A. M. Stoneham, *Making tracks: electronic excitation roles in forming swift heavy ions*, J. Phys.: Condens. Matter **21**, 474205 (2009).

97. R. L. Fleischer, P. B. Price, and R. M. Walker, *Ion Explosion Spike Mechanism for Formation of Charged-Particle Tracks in Solids*, J. Appl. Phys. **36**, 3645 (1965).

98. E. M. Bringa and R. E. Johnson, *Coulomb Explosion and Thermal Spikes*, Phys. Rev. Lett. **88**, 166501 (2002).

99. M. Toulemonde, C. Dufour, and E. Paumier, *Transient thermal process after a high-energy heavy-ion irradiation of amorphous metals and semiconductors*, Phys. Rev. B **46**, 362 (1992).

100. A. Meftah, J. M. Costantini, N. Khalfaoui, S. Boudjadar, J. P. Stoquert, F. Studer, and M. Toulemonde, *Experimental determination of track cross-section in $Gd_3Ga_5O_{12}$ and comparison to the inelastic thermal spike model applied to several materials*, Nucl. Instrum. Meth. Phys. Res. B **237**, 563 (2005).

101. S. Klaumünzer, *Ion tracks in quartz and vitreous silica*, Nucl. Instrum. Meth. Phys. Res. B **225**, 136 (2004).

102. M. P. R. Waligórski, R. N. Hamm, and R. Katz, *The Radial Distribution of Dose around the Path of a Heavy Ion in Liquid Water*, Nucl. Tracks Radiat. Meas. **11**, 309 (1986).

103. G. Hobler and G. Betz, *On the useful range of application of molecular dynamics simulations in the recoil interaction approximation*, Nucl. Instrum. Meth. Phys. Res. B **180**, 203 (2001).

104. F. Gao, D. Chen, W. Hu, and W. J. Weber, *Energy dissipation and defect generation in nanocrystalline silicon carbide*, Phys. Rev. B **81**, 184101 (2010).

105. N. Swaminathan, P. J. Kamenski, D. Morgan, and I. Szlufarska, *Effects of grain size and grain boundaries on defect production in nanocrystalline 3C-SiC*, Acta Mater. **58**, 2843 (2010).

106. B. Johannessen, P. Kluth, D. J. Llewellyn, G. J. Foran, D. J. Cookson, and M. C. Ridgway, *Amorphization of embedded Cu nanocrystals by ion irradiation*, Appl. Phys. Lett. **90**, 073119 (2007).

107. S. Dhara, *Formation, Dynamics, and Characterization of Nanostructures by Ion Beam Irradiation*, Crit. Rev. Solid State Mater. Sci **32**, 1 (2007).

108. J. G. Zhu, C. W. White, J. D. Budai, S. P. Withrow, and Y. Chen, *Growth of Ge, Si, and SiGe nanocrystals in SiO_2 matrices*, J. Appl. Phys. **78**, 4386 (1995).

109. K.-H. Heinig, B. Schmidt, M. Strobel, and H. Bernas, *Inverse Ostwald Ripening and Self-Organization of Nanoclusters due to Ion Irradiation*, MRS Proceedings **650**, R9.6/O14.6 (2000).

110. G. C. Rizza, M. Strobel, K. H. Heinig, and H. Bernas, *Ion irradiation of gold inclusions in SiO_2: Experimental evidence for inverse Ostwald ripening*, Nucl. Instrum. Meth. Phys. Res. B **178**, 78 (2001).

111. K. Nordlund and R. S. Averback, *Point defect movement and annealing in collision cascades*, Phys. Rev. B **56**, 2421 (1997).